Leachate of the Brukunga Mine Site – A Reactive Modelling Study

by

Joshua Edwards

Thesis
Submitted to Flinders University
for the degree of

Master of Science (Groundwater Hydrology)

College of Science and Engineering

November 2018

Table of Contents

List of Abbreviations

AMD	Acid Mine Drainage
km	kilometres
SA	South Australia
REDOX	Reduction oxidation reactions
WR	Waste rock
SO_4^{2-}	Sulfate
Fe	Iron
Al	Aluminium
FeS_2	Pyrite
$CaCO_3$	Calcite
wt.%	weight percent
ha	hectares
D.O	Dissolved oxygen
Fe^{2+}	Ferrous iron
Fe^{3+}	Ferric iron
ALD	Anoxic limestone drain
FeS	Pyrrhotite
$FeAsS$	Arsenopyrite
$CuFeS_2$	Chalcopyrite
$(ZnFe)S$	Sphalerite
PbS	Galena
Mt	Million tonnes
m	meters
TAG	Technical Advisory Group
PRISA	Department of Primary Industries and Resources South Australia
cm	centimetres
kg	kilograms
mL	millilitres

L	litres
ORP	oxidation reduction potential
EC	electrical conductivity
S_T	Total sulfur
ASS	Acid Sulfate Soils
S_{Cr}	Chromium reduceable sulfur
S_{KCl}	KCl extractable sulfur
S_{HCl}	HCl extractable sulfur
S_{TOS}	Total Oxidisable sulfur
S_{NAS}	Net Acid soluble sulfur
ANC	Acid Neutralising Capacity
Ca^{2+}	Calcium
Na^{+}	Sodium

List of Figures

List of Tables

List of Equations

Chapter 1 Introduction

Mining has drastic impacts on the environment both visually and physically, with limited long-term treatment and remediation options available on a global scale. Acid Mine Drainage (AMD) and the leachate that is produced is a major physical and visual impact that is a result from past and current mining activities (Johnson and Hallberg, 2005). This has been known to impact areas some extent from the initial source of leachate on site, with ranges been up to 10's of kilometres (km) from the initial source (F Taylor and C Cox, 1980, Cox et al., 2006). In South Australia (SA) the Brukunga Mine site is a prime study ground for investigating in identifying suitable long-term treatment options for AMD and leachates from pyrite mine sites (F Taylor and C Cox, 1980, Cox et al., 2006, McLeary, 2009). Production of leachate arises from exposing large quantities of minerals to geological processes; weathering and reduction oxidation reactions (REDOX) (Akcil and Koldas, 2006, Johnson and Hallberg, 2005, Blowes et al., 2003). The exposure of these leachate producing minerals, may be through waste rock (WR) piles or tailings and tailings storage facilities, which is the current situation at Brukunga mine site, other mining activities may also result in the production of leachate been produced both throughout the duration of the life of the mine and post mining operations.

Past mining activities and management at the Brukunga mine site has resulted in environmental degradation and impact. Currently groundwater and surface water in the immediate vicinity of the quarry bench, WR piles and tailings storage facility has water quality parameters typical of AMD, with severely reduced pH, mobilisation of heavy metals, elevated Sulfate (SO_4^{2-}), Iron (Fe) and Aluminium (Al) (Johnson and Hallberg, 2005, Akcil and Koldas, 2006, Garcia et al., 2005, Jurjovec et al., 2002). Historically there has been several releases of leachate in to the Dawesley creek, impacting surface waters as far as Lake Alexandria, some 40 km to the south of the site.

Primarily investigating the REDOX reactions of Pyrite (FeS_2), it has been proposed that burial and permanent saturation of WR and tailings material to eliminate REDOX processes may be a viable long-term remediation option. Initial testing identified that the formation of secondary minerals Jarosite and the subsequent latent REDOX processes of this mineral and FeS_2 would still produce enough leachate to affect the cover water and surrounding material in the area (Devlopment, 2013). Blending of calcite ($CaCO_3$) with the WR and tailings material was proposed to counteract this latent REDOX reaction, through the dissolution of $CaCO_3$ and subsequent increase of pH resulting in an overall improved water quality of the leachate. A series of column tests was conducted to identify the most appropriate weight percent (wt.%) of material to provide a suitable long-term solution at the Brukunga mine site (Devlopment, 2013). This current study aims to model the column tests that were conducted and reproduce the results observed, identifying the driving reactions that govern the leachate at the Brukunga mine site and the evolution of the neutralisation process. This reactive modelling study will facilitate in ascertaining the longevity of the proposed solution. Several stages were carried out to achieve this objective, 1) analysis of the data provided from column tests conducted, 2) establish a working flow model that replicates the volumes of leachate collected at appropriate sampling times; and 3) introduce appropriate quantities of minerals from static geochemical tests and geochemical reactions to closer simulate processes occurring in the columns.

Chapter 2 Literature Review

Environmental sustainability is an ever-growing critical issue in many areas of industry, as there are many different processes, both manmade and natural, that can alter the environment in an

unfavourable way. Industrial operations, such as scrubbing of flue gases in power stations (Johnson and Hallberg, 2005) may produce AMD, it can also be a naturally occurring phenomena, however, mining of minerals and resources is the largest cause of AMD worldwide (Kefeni et al., 2017, Blowes et al., 2003). AMD at mine sites occurs during operations but it is largely through the resultant state the site is left in that is the largest influence to the production of AMD. The production of AMD is though a process by which sulphide bearing minerals are oxidised; typically resulting in reduced pH and mobilising heavy metals and other toxins, normally contained as immobile trace elements in the environment (Akcil and Koldas, 2006) as shown in **Table 1**. This process causes many long-term issues that persist for decades and can be extremely detrimental to the environment and human health (Akcil and Koldas, 2006, Johnson and Hallberg, 2005, Shabalala et al., 2017, Kalyoncu Erguler et al., 2014, Blowes et al., 2003). Runoff produced as a results from AMD may smother aquatic life in streams and rivers which can compound further up the food chain affecting not only flora but local fauna (Kefeni et al., 2017). These contaminated waters in many cases can exceed the thresholds for irrigation and livestock.

Table 1. List of heavy metals that are most likely found in Acid Mine Drainage from mine sites. Other heavy metals may be present, though this is dependent on the environment and varies from site to site.

List of potential heavy metals in AMD	
Iron (Ferric and Ferrous)	Fe
Aluminium	Al
Magnesium	Mg
Zinc	Zi
Copper	Cu
Chromium	Cr
Cobalt	Co
Manganese	Mn
Lead	Pb
Nickel	Ni
Cadmium	Cd
Vanadium	V

Johnson and Hallberg (2005) outlined that in 1989 there was 19,300 km of streams and rivers, and 720 km^2 of lakes and revivors that were seriously damaged due to AMD. Not included is the amount of groundwater that may have been contaminated, although this figure is quite old, it dose highlight the damaging effect AMD has globally. Because of the nature of AMD if is very difficult to properly asses (Johnson and Hallberg, 2005), as the process may continue for many years after the mine has be closed, such as the Brukunga Pyrite Mine in SA. Ongoing effects of AMD may be due to rebounding water levels from groundwater and surface water being restored to pre-mining conditions, along with other hydrogeochemical reactions that may occur as a result of this. There are many sources of AMD at a mine site, and each must be assed and managed properly to minimise the impact, a list of possible mine site sources, both during and post operations, is shown in **Table 2**. Of these possible sources, rock dumps and tailing impoundments are the largest contributors due to their sheer volume, and most research is focused around treatment and remediation of these.

Table 2. Sources of AMD at a mine site, this is split into primary and secondary sources. (Akcil and Koldas, 2006)

Primary source	**Secondary source**
Mine rock dumps	Treatment of rock ponds
Tailing impoundments	Rock cuts

Underground and open pit mine works	Concentrated load out
Pumped/nature discharged underground water	Stockpiles
Diffuse seeps from replaced overburden in rehabilitated areas	Concentrate spills along roads
Construction rock used in roads, dams, ect.	Emergency ponds

As a result, there have been many studies into the processes and governing reactions of AMD and resultant leachate that is produced, particularly FeS_2 as this is the primary mineral responsible. Although there are many different sulphide bearing minerals, the processes are best examined though the REDOX reactions of FeS_2 (Akcil and Koldas, 2006). The oxidation of FeS_2 by dissolved oxygen (D.O) is shown through **Equation 1** (Kefeni et al., 2017, Appelo and Postma, 2005). This produces ferrous iron (Fe^{2+}), two $SO_4^{2-}$and two hydrogen ions, which unless neutralised will reduce the pH of the environment. However as Fe^{2+} is released this may also, in turn become oxidised through the reactions in **Equation 2** resulting in ferric iron (Fe^{3+}) (Kefeni et al., 2017, Appelo and Postma, 2005). Fe^{3+} can also act as an oxidant for FeS_2 as show in **Equation 3** (Kefeni et al., 2017, Appelo and Postma, 2005). The overall products produced from this reaction are 15 Fe^{3+}, two $SO_4^{2-}$and 16 hydrogen ions. The oxidation of FeS_2 by Fe^{3+} is many times faster than by dissolved oxygen and quantity of products released are significantly greater. Although it may not be evident at the start, the main oxidant of FeS_2 is Fe^{3+}, and D.O is the driving force that maintains this process through the reaction shown in **Equation 2**. As the oxidation of FeS_2 releases hydrogen ions which if not neutralised reduce the pH, subsequently mobilising heavy metals present in the surrounding material. Increasing the pH of the leachates can cause these heavy metals in solution to do one of the following; sorb, complex to surfaces or precipitate out of suspension.

Equation 1: $$FeS_2 + 7/2\,O_2 + H_2O \rightarrow Fe^{2+} + 2SO_4^{2-} + 2H^+$$

Equation 2: $$Fe^{2+} + 1/4\,O_2 + H^+ \rightarrow Fe^{3+} + 1/2\,H_2O$$

Equation 3: $$FeS_2 + 14Fe^{3+} + 8H_2O \rightarrow 15Fe^{2+} + 2SO_4^{2-} + 16H^+$$

Due to this fact, many of the remediation and treatment options available deal with increasing pH rendering heavy metals immobile due to sorption, complex to surfaces or precipitation. Two different categories of treatment are available, active and passive. Prevention methods are also viable, though for this to be successful prevention should be achieved prior to the commencement of mining activities. Prevention methods may include applications of organic wastes, altering the hydrology, inundation, bactericides and coatings of the sulphide mineral to prevent oxidation (Evangelou, 1998). As shown above, in **Equations 1-3** and **Figure 1**, the oxidation of FeS_2 involves both oxygen and water, limiting or eliminating one of these two key ingredients would prevent oxidation of FeS_2 and other sulphide minerals, which is the key aim of prevention methods. The two categories of treatment methods – active and passive – both achieve the neutralisation of pH, minimisation of heavy metals, through adsorption, absorption and precipitation, along with the reduction in sulphate though physical, biological and chemical processes (Taylor et al., 2005, Kefeni et al., 2017). Active treatment options involve a constant and regular dosing of reagent for operation, while passive treatment options only require occasional inputs or maintenance (Taylor et al., 2005). There are several different types of passive treatment options that area available, these can be seen in **Table 3** (Taylor et al., 2005) these include wetlands, phosphatic material, alkaline material and anoxic limestone drains (ALD) (Evangelou, 1998).

Table 3. Passive treatment options that are available (Evangelou, 1998, Taylor et al., 2005)

Passive Treatment Methods	
Open Limestone Drains (OLD)	Successive Alkalinity Producing Systems (SAPS)
Anoxic Limestone Drains (ALD)	Permeable Reactive Barriers (PRB)
Limestone Diversion Wells (LDW)	Slag Leach Beds (SLB)
Pyrolusite Limestone Beds	Microbial Reactor System (MRS)
Aerobic and anaerobic wetlands	Sulphide passivation compounds
Reverse Alkalinity Producing Systems (RAPS)	Alkalinity producing covers
Vertica Flow Wetlands (VFW)	Gas Redox and Displacement System (GaRDS)
Alkalinity Producing Systems (APS)	Electrochemical covers

There is no one passive treatment option that is superior over the rest, however passive treatments are used in post mine closure and selection is site specific, determined though the geology and minerology of the area and the end use of the water. Unlike passive treatments there is only two different active treatment options, in-situ and fixed plant systems (Taylor et al., 2005).

Fixed plant systems are used in active mine sites and post closure. In situ systems are portable systems generally used to raise the pH of waterbodies at the specific site. Fixed plant systems can be engineered to handle and accommodate all types of AMD water in any location (Taylor et al., 2005, Kefeni et al., 2017). However, Komnitsas et al. (2004) highlights that fixed plant systems do involve a high capital and operating costs, as is shown at Brukunga mine site, where the annual operating costs for the site are $550 000 per annum (F Taylor and C Cox, 1980, Cox et al., 2006). Other concerns with active treatment options is the need for long term maintenance and the potential for development of secondary hazardous materials (Komnitsas et al., 2004). Many treatment options, both passive and active, involve the addition of neutralisation minerals such as calcium carbonate/$CaCO_3$ or agricultural lime, amongst other neutralising agents, see **Table 4**, to increase the pH. The current treatment options used at the Brukunga Mine Site is an active fixed plant system, with research and trials going into passive systems, similar to that of an ALD passive system. Of all the current treatment options available, there is no treatment that is a complete 'walk away' solution for AMD, continual maintenance and monitoring needs to be conducted to ensure that the desired outcome is achieved and maintained to promote environmental stability in the area (Taylor et al., 2005, Komnitsas et al., 2004, Johnson and Hallberg, 2005). As such, each case of AMD is unique to each site, based on the geology, minerology and hydrology of the area. Therefore, the treatment options selected are done so with this in mind and the desired outcome of the end use of the discharge waters (Kalin et al., 2006, Cravotta III and Trahan, 1999).

Table 4. A list of the current neutralisation materials available to be used in the treatment of AMD (Taylor et al., 2005)

Neutralisation Materials	
Limestone $(\boldsymbol{CaCO_3})$	Sodium carbonate (Na_2CO_3)
Quicklime $(\boldsymbol{CaO})$	Sodium Hydroxide $(NaOH)$
Hydrated lime $(\boldsymbol{Ca(OH)_2})$	Ammonia (NH_3)
Dolomite $(\boldsymbol{CaMg(CO_3)_2})$	Potassium Hydroxide (KOH)
Magnesite $(\boldsymbol{MgCO_3})$	Calcium peroxide (CaO_2)
Caustic magnesia $(\boldsymbol{MgO})$	Barium carbonate $(BaCO_3)$
Lime kiln dust $(\boldsymbol{CaO, CaCO_3})$	Barium hydroxide $(Ba(OH)_2)$

Fly-ash (Ca, Mg, Na, K oxides and hydroxides)	Fluidised bed ash (Ca, Mg, Na, and K oxides and hydroxides

Column tests are a means of studying AMD without further adding to the deterioration of the environment, with the added advantage of gaining insight to processes that control AMD. Column tests monitor the evolution and quality of water that the waste material been tested leaves behind due to weathering processes, these are conducted in laboratory conditions, in a way that can represent natural field weathering processes (Garcia et al., 2005, Kalyoncu Erguler et al., 2014). As such there has been several studies into the influence of the column size used and the results obtained. Kalyoncu Erguler et al. (2014) and Garcia et al. (2005) both noted that the column size, height, diameter, volume and particle size are the determining factors that contributes to weathering processes, however oxidation is slower in larger columns. Garcia et al. (2005) concluded that medium size columns give excellent results in an adequate time frame.

This image has been removed due to copyright restrictions. Available in the following textbook: *Geochemistry, Groundwater and Pollution*, (Appelo and Postma, 2005)

Figure 1. Schematic diagram of the possible oxidation pathways of pyrite (Appelo and Postma, 2005)

Modelling of column test can be extremely beneficial in identifying governing processes that drive AMD and leachate, along with quantifying the results of column tests. Though this is extremely difficult as there is an apparent oversimplification of the conceptual model and a lack of input data available to constrain column test models (Jasna et al., 2004). However, there has been many successful models constructed in numerous programs of column and batch reactor tests. Program selection is based on the type of modelling to be conducted. Shabalala et al. (2017) used Geochemists Workbench to identify mineral precipitates and advective transport to validate findings from column test conducted on mineral precipitation and speciation.

Equation 4: $$r = 10^{-8.19} m_{O_2}^{0.5} m_{H^+}^{-0.11} \ (mol/m^2/s)$$

Equation 5: $$r = 10^{-6.07} m_{Fe^{3+}}^{0.93} m_{Fe^{2+}}^{-0.40} \ (mol/m^2/s)$$

Equation 6: $$r = 10^{-8.58} m_{Fe^{3+}}^{0.3} m_{Fe^{2+}}^{-0.47} m_{H^+}^{-0.32} \ (mol/m^2/s)$$

Komnitsas et al. (2004) and Jasna et al. (2004) used the program PHREEQC to model both the neutralising and buffering reactions that affect the pH during AMD. Jasna et al. (2004) also used several rate constants and expressions that were determined prior to the modelling, these were added into the MINTEQA2 database. Another study by Miller et al. (2013) used the PHREEQC modelling program to identify zinc and nickel removal though sorption with Fe precipitates. Identifying the rate expression of FeS_2 in modelling AMD is key, however, as stated previously, each case of AMD is specific to its location, geology, minerology and crystal size (Taylor et al., 2005, Evangelou, 1998, Appelo et al., 1998, Kalyoncu Erguler et al., 2014). The overall redox pathways for FeS_2 are shown in **Figure 1**. Three rate expressions have been developed by Williamson and Rimstidt (Appelo and Postma, 2005), shown in **Equations 4-6**, which have been used and studied extensively.

Chapter 3 The Brukunga Mine Site and Legacy Mines in Australia

As the results of mining is one of the primary causes of AMD, identifying mines both past and present that are producing AMD is extremely important. Since the 1990's mining has been advancing

to embrace sustainable development, however mining processes and technologies are less developed in regards to environmental considerations than other industries such as forestry, fisheries and agriculture (Worrall et al., 2009). Mining and mining processes are generally more visible, highlighted by the large areas and visual impact that is produced compared to the other industries mentioned. Particularly historical mine sites that have been abandoned, are derelict or orphaned are common in Australia due to its long mining history and are referred to as Legacy Mine Land (Worrall et al., 2009). Legacy mine land has a range of issues associated with it, from unclear or disputed ownership, to land alteration to various degrees (minor to catastrophic) to questions over future land use based on past activities (Worrall et al., 2009). Typically, historical mining procedures and practices are regarded as unsatisfactory, in regards to the environment and processes used, mines were naturally abandoned when finished and no priority was given to any environmental concerns (Worrall et al., 2009). Globally, Legacy Mine Land and sites are a significant and pressing issue, with limited published research in this area (Worrall et al., 2009). The availability of information and documentation on Legacy Mines around the world ranges from very poor to good as shown in **Table 5**. Within Australia, Legacy Mines are a very prominent issue, with approximately 32,600 sites Australia wide, however the information on the number of Legacy sites in Australia is quite poor as shown in **Table 6**.

Table 5. Number of legacy mine sites and quality of information available globally (Worrall et al., 2009).

Country	Approx. number of sites	Information Quality
USA	600000+	Poor
Canada	10100	Good
UK	11700	Average
South Africa	8000	Average
Sweden	1000	Good
Japan	5500	Good
Rest of World	Likely millions	Very poor

Table 6. Number of legacy mine sites and quality of information available within Australia and each state/territory (Worrall et al., 2009).

State or Territory	Approx. number of sites	Information Quality
Australian Capital Territory	Unknown	Poor
New South Wales	570	Poor
Northern Territory	Unknown	Poor
Queensland	15000	Average
South Australia	4000	Average
Tasmania	30	Average
Victoria	2000	Average
Western Australia	11000	Average
Total	32600+	

In SA there are approximately 4000 Legacy Mine Land sites with Brukunga Mine Site being one. The Brukunga Mine site is located approximately 47km east of Adelaide and 4 km north of Narine in the Mount Lofty ranges (see **Figure 2**) (F Taylor and C Cox, 1980, Uvarova et al., 2016).

This image has been removed due to copyright restrictions. Available online from [https://www.sciencedirect.com/science/article/pii/S037567421630190X]

Figure 2. Location of Brukunga Mine site in South Australia, in relation to Adelaide (Uvarova et al., 2016))

The geological formation that hosts the minerals of interest in the area is from the Narine pyrite member of the Kanmantoo Group ((Parker, 1986, Pollock et al., 2018, PRISA, 2005). The Narine Pyrite member is a sulphide rich horizon consisting of several beds extending approximately 100km north and south above ground, as well as extending below the surface (Uvarova et al., 2016, PRISA, 2005). Being a major source of sulfur, several sulfur rich minerals are present in the area, primarily FeS_2 and Pyrrhotite (FeS), though Arsenopyrite ($FeAsS$), Chalcopyrite ($CuFeS_2$) and Sphalerite ($(ZnFe)S$) and Galena (PbS) are also recorded as being present (F Taylor and C Cox, 1980). Due to these sulphide rich minerals in the area the Brukunga Pyrite Mine was established in 1955 to provide a source of sulfur for superphosphate, this venture was operated by Narine Pyrites Pty Ltd with closure of the mine occurring in 1972 (PRISA, 2005). The extent of the Brukunga mine site was spread across a 123 ha area (F Taylor and C Cox, 1980, PRISA, 2005) which included a small creek – Dawesley Creek – that passed through the mine site. The mining operations produced 8 Million tonnes (Mt) of WR and 3.5 Mt of Tailings (F Taylor and C Cox, 1980, Cox et al., 2006, PRISA, 2005) these were stored in two large WR piles and a tailings storage facility (see **Figure 3**).

This image has been removed due to copyright restrictions. Available online from [https://www.google.com/maps/search/Brukunga+mine/@-35.0046666,138.9400861,1894m/data=!3m1!1e3]

Figure 3. Map of the Brukunga pyrite mine site. WR piles are located to the north west and south west. The tailings storage facility is located to the east. (google maps – image of Brukunga mine site accessed on 29/7/2018)

Post closure Dawesley creek was diverted, this occurred following the burial of old creek channels during operation (F Taylor and C Cox, 1980). Water from Dawesley creek has been found to be unsuitable for use 20 km downstream form the mine site, as Dawesley Creek feeds the Bremmer river which in turn discharges into Lake Alexandria, remediation and neutralisation of AMD discharge from the site is crucial (F Taylor and C Cox, 1980, Cox et al., 2006). As the large WR piles are well aerated and include large amounts of surface area due to the size of the material, pyrite and subsequently produced jarosite, can be oxidised throughout the WR pile in substantial quantities (F Taylor and C Cox, 1980). F Taylor and C Cox (1980) outlined a study EGi, 1995, that identified that 65% of AMD that was generated from the Brukunga Mine Site was produced due to the oxidation of WR piles and was discharged into Dawesley Creek. The Tailings storage facility was used early in the post closure as a ponding area for AMD evaporation. However, this concentrated the AMD through recycling and evapo-concentration of contaminates and a lime neutralisation plant was installed to help treat wastewater and AMD from the tailings storage facility (F Taylor and C Cox, 1980). The quarry bench was left exposed post closure as shown in **Figure 3**, this consisted of two large walls approximately 1.8 km long and 75-80 meters (m) high (F Taylor and C Cox, 1980, Cox et al., 2006, PRISA, 2005), oxidation of this quarry bench has led to an increased volume of naturally occurring AMD in the area. The Australian Nuclear Scientific & Technological Organisation have estimated that the combination of naturally occurring oxidation along with the AMD leachate from the WR piles and

tailings storage facility would facilitate acid forming reactions for 240-750 years if left untreated (Cox et al., 2006, PRISA, 2005). Although the Brukunga mine site is not the only legacy mine land in the area, it is highlighted and classified as a major source of AMD due to the mentioned issues and history of the site (F Taylor and C Cox, 1980). However, there has been no previous studies of the Brukunga mine site and surrounding area pre-mining, resulting in no baseline, giving rise to unknown contributions from potentially unknown sources of AMD in the area (F Taylor and C Cox, 1980). To prevent any further damage and halt the release of AMD leachate form the site several projects have been initiated to identify the best course of action, including this current study as part of a larger remediation porject.

Chapter 4 Column Test and Data Analysis

4.1. Column Test Setup

4.1.1 Overview

The column tests conducted at the Brukunga mine site are part of a larger, long-term project initiated by the Technical Advisory Group (TAG), established by Department of Primary Industries and Resources South Australia (PIRSA) (Devlopment, 2013). The TAG consisted of international experts in AMD (Devlopment, 2013) , with the overall aim of the project to identify and implement a 'walk away' solution in the Brukunga mine site. Although as stated above in **Chapter 2**, currently, there are no treatment options available that is a complete 'walk away' solution, and as such continual maintenance is required (Johnson and Hallberg, 2005). However, research into minimising the amount of maintenance and capital need to initiate a solution and ensuring that the solution works with minimal ongoing maintenance and capital is a step in the right direction. The TAG developed a treatment option which involves the burial and permanent saturation of the co-disposed material, consisting of WR and tailings, to eliminate oxidation and thus the generation of acidity through REDOX processes. However, it was noted that secondary dissolution of the mineral jarosite would result in acidity generation. Therefore, it was proposed that an adequate neutralising material should be blended with the co-disposed material to reduce and mitigate the produced acidity from secondary dissolution. To identify the amount of neutralising material required with the appropriate amount of co-disposed material to fulfil this treatment option, five stages of test work were proposed, of which three have been completed to date. Outlined below are the stages and the status of each (Devlopment, 2013),

- Stage 1 Column leach test work (Completed)
- Bulk leach test work (Completed)
- Stage 2 Column leach test work (Completed)
- Stage 3 Presentation trail (In progress)
- Stage 4 Large scale field trail (Not yet started)

Stage 1 column leach test work: The Stage 1 column leach test work was completed to identify the efficiency and effectiveness of a water cover and 1 wt.% addition of $CaCO_3$ blended with the co-disposed material (Devlopment, 2013). Results showed that a larger wt.% of $CaCO_3$ would be required, as the secondary mineral jarosite provided enough latent acidity though dissolution and possibly other forms of oxidation to affect both the water cover and the column.

Bulk leach test work: Bulk leach test work was completed to identify the optimal mixture of wt.% WR, tailings and $CaCO_3$. Results identified that 60 wt.% WR, 36 wt.% tailings and 4% $CaCO_3$ was the optimal blend to achieve the neutralisation of the acidity produced by the dissolution of jarosite.

Stage 2 Column leach test work: Stage 2 Leach test work was completed to identify if the ideal co-disposed material mixture would neutralise the acidity of the leachate and not affect the water cover under static conditions (Devlopment, 2013).

Stage 3 Presentation trial: Stage 3 presentation trial is a small-scale field test involving 40 tonnes of co-disposed material blended with 4 wt.% $CaCO_3$ which is currently in progress. The major objectives of the Stage 3 presentation trial are identification of practical methods for irrigation, drying and construction issues that are associated at field scales of this size.

Stage 4 Large scale field trial: Is an upscaling of the presentation trail to 10,000 tonnes building on information obtained from Stage 3 presentation trial.

This project focuses on the Stage 2 column leach test work which has been built on information obtained from, Stage 1 Column leach test work and Bulk leach test work. Modelling of the Stage 2 column leach test work will assist in quantifying the results and identify the driving reactions and mechanisms at the Brukunga mine site. This will identify the long-term viability of the proposed 'walk away' solution.

4.1.2 Column Setup and Sampling Procedure

The stage 2 leachate test work was conducted using 12 columns, one column was a control which contained WR and tailings with no added $CaCO_3$, while the other 11 contained various mixtures of WR, tailings and $CaCO_3$ (see **Table 7**). The column design is shown in **Figure 4**, the preparation and setup of each column was completed as follows;

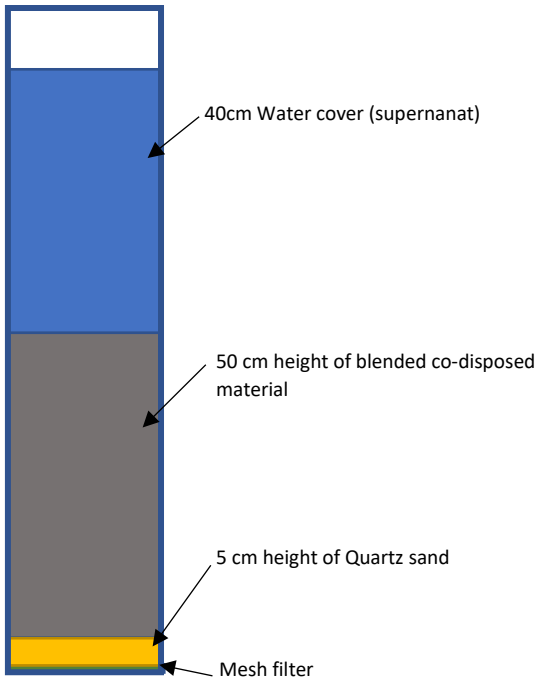

Figure 4. Design setup of the columns.

Each column consisted of a clear *Perspex* pipe with an internal diameter of 19 centimetres (cm). At the base a valve was installed to control the leachate discharge during sampling, the inside of the base was lined with a fabric mesh filter. Two kilograms (kg) of pure quartz sand was placed on top of the fabric mesh filter resulting in approximately a five (5) cm deep quartz layer. Next, co-disposed material was place in the column up to a height of 50 cm. This was done gently as not to disturb the quartz sand and fabric mesh filter. Then Dawesley creek water was used to irrigate the column, this was done rapidly from the top of the column with the valve closed at the base, irrigation continued until a water cover of 40 cm above the co-disposed material was obtained. This was left to stand for five days before initial sampling commenced.

Table 7. The ratios of the blended material in each of the columns used in the column leach trial testwork, this is presented as a wt.% fraction.

Column ID	Waste Rock Fraction %	Tailings Fraction %	Added Limestone Fraction %
Mix_0	63	37	0
Mix_2	62	36	2
Mix_4	60	36	4
Mix_6A	59	35	6
WR_2	98	0	2
WR_4	96	0	4
WR(4)_2	98	0	2
WR(4)_4	96	0	4
WR(1.2)_2	98	0	2
WR(1.2)_4	96	0	4
T2	0	98	2
T4	0	96	4

The sampling procedure and frequency is outlined below;

Sampling of the columns can be split into two distinct sections, the supernatant and leachate, with the leachate been the focus of this study. Sampling of the supernatant is done first with in situ field measurement taken. Following in situ field measurements a supernatant sample of approximately 300 millilitres (mL) is obtained. For leachate sampling the tap was opened at the base of the columns. Leachate was allowed to drain freely until approximately 1.5 litres (L) was obtained. Sampling times were not recorded for the leachate, though it is noted that leachate sampling took between 30 minutes to 4 hours, ex-situ field measurements of pH, oxidation reduction potential (ORP), electrical conductivity (EC) and acidity were taken during this time. Following sampling the column was irrigated with water from Dawesley Creek equal to the combined volume of the supernatant and leachate samples. Samples taken from Stage 2a were sent to Eurofins | MGT Environmental Laboratories for analysis. This was repeated on a weekly basis for nine weeks. Stage 2b ran for six weeks using ALS Laboratories for the analysis of the samples taken. Results from the laboratory analysis can be view in **Appendix A**.

Reasoning for the change of laboratories conducting the analysis was due to inconsistencies of laboratory analytical data (Devlopment, 2013). It is also noted that the analysis suite changed slightly

from Eurofins | MGT to ALS Laboratories. The changes in the analysis included the following; chloride, fluoride, arsenic, cadmium, chromium, lead and zinc.

4.1.3 Composition of Co-Disposed Material and Creek Water

Water from Dawesley Creek, $CaCO_3$ along with tailings and WR material were all subjected to analysis prior to test work. This was completed to obtain static bulk chemistry of major elements and selected trace elements (Devlopment, 2013). Along with bulk chemistry, several key environmental geochemical parameters were also analysed for the WR, tailings and $CaCO_3$. These parameters help with identifying the key minerals that may be present in the material. These Key minerals may assist in the neutralisation of acid or facilitate the release of acid, either reducing or increasing AMD leachate produced. A list of the parameters is shown in **Table 8** followed by a description of each geochemical parameter.

Table 8. Parameters used to test the Dawesley Creek water and geochemical paramters used for analysis of the waste rock and tailings used in the columns. Detection limits are shown in brackets. (Devlopment, 2013)

Dawesley Creek Water parameters	Waste rock and Tailings geochemical Parameters
pH	Gravimetric Moisture Content (GMC)
EC (100uS/cm)	Total Sulfur (0.1 wt.% S)
Acidity and Alkalinity (10mg/L CaCO3)	Chromium Reducible Sulfur (0.1 wt.% S)
Ca, K, Mg, Na (1mg/L)	KCl-Extractable Sulfur (0.1 wt.% S)
AL (0.05mg/L), Cu (0.001mg/L), Fe (0.01mg/L), Mn (0.001mg/L), Ni (0.005mg/L)	HCl-Extractable Sulfur (0.1 wt.% S)
SO4 (1mg/L)	Acid Neutralisation Capacity (ANC) (1kg/t H2SO4)
	Net Acid Generation (NAG) (1kg/t H2SO4)

Total sulfur (S_T): *This geochemical test is a measure of the maximum risk that may eventuate though the oxidation of sulfate soils and minerals (Ahern, 2004, Devlopment, 2013). As the S_T is a measure of the maximum risk from Acid Sulfate Soils (ASS) it is widely used in the mining sector. This maximum risk, however, is based on the stoichiometry of FeS_2 as shown in **Equation 7** below. If gypsum is present in appreciable quantities, this can lead to an overestimation of maximum risk and subsequently to inappropriate treatment of the waste (Ahern, 2004, Devlopment, 2013).*

Equation 7: $$FeS_2 + {}^{15}/_{4}\, O_2 + {}^{7}/_{2}\, H_2O \rightarrow Fe(OH)_3 \downarrow + 2SO_4^{2-} + 4H^+$$

Acid neutralising material and actual acidity are not accounted for in this test and other measurements need to be made for these (Ahern, 2004, Devlopment, 2013).

Chromium reduceable sulfur (S_{Cr}): *this test provides a determination of the reduced inorganic sulfur that has not been subjected to any interference from other SO_4^{2-}sources, such as organic suflur and SO_4^{2-}minerals such as gypsum and anhydrite (Ahern, 2004, Devlopment, 2013). Typically, it is a measure of the following;*

- *Pyrite*
- *Iron disulfides*
- *Elemental sulfur*
- *Acid volatile sulphides*

- *Thiosulfate*
- *Tetrathionate*
- *Polythionates*

KCl extractable sulfur (S_{KCl}): *this geochemical test recovers the soluble and exchangeable SO_4^{2-} that is in the sample as readily soluble SO_4^{2-} minerals by sulfuric acid, such as gypsum and anhydrite (Ahern, 2004, Devlopment, 2013). This can be used in conjunction with HCl extractable sulfur for estimations of the net acid soluble sulfur (S_{NAS}) as shown though* ***Equation 8****.*

Equation 8: $$S_{NAS} = S_{HCl} - S_{KCl}$$

HCl extractable sulfur (S_{HCl}): *this geochemical test provides a measurement of soluble and exchangeable SO_4^{2-} in the sample. This is different to S_{KCl} in that this sulfate is from realtivily insoluble iron and aluminium hydroxyl-sulfate compounds (Ahern, 2004, Devlopment, 2013). Overall this measurement provides a measure of the amount of jarosite and natrojarosite in the sample (Ahern, 2004, Devlopment, 2013).*

Total Oxidisable sulfur (S_{TOS}): *is the calculated difference between the S_T and the S_{HCl} as shown in* ***Equation 9****;*

Equation 9: $$S_{TOS} = S_T - S_{HCl}$$

This is a conservative measurement and a low-cost determination of FeS_2 in a sample (Ahern, 2004, Devlopment, 2013). However, this measurement doesn't give the actual acidity of the sample and as this measurement is conservative in nature, S_{Cr} measurement may result in more adequate results leading to treatment options more suitable for the situation.

Net Acid soluble sulfur (S_{NAS}): *this is a measurement of the acidity that is retained in the material, usually as jarosite or natojarosite as shown in* ***Equation 10*** *and* ***Equation 11*** *(Ahern, 2004, Devlopment, 2013).*

Equation 10: $$KFe_3(SO_4)_2(OH)_6 + 3H_2O \rightarrow Fe(OH)_3 \downarrow + 2SO_4^{2-} + 3H^+ + K^+$$

Equation 11: $$NaFe_3(SO_4)_2(OH)_6 + 3H_2O \rightarrow Fe(OH)_3 \downarrow + 2SO_4^{2-} + 3H^+ + Na^+$$

This is obtained thought removing the readily soluble sulphate minerals from the relatively insoluble iron and aluminium hydroxyl sulphate compounds as shown above in ***Equation 8****;*

Acid Neutralising Capacity (ANC): *this geochemical test is a measure of the ability of the soil to buffer the acidity and limit the lowering of the soil pH thought the dissolution of calcium and magnesium carbonates, cation exchange reactions, and reactions with clay and organic fractions present in the soil matrix (Ahern, 2004, Devlopment, 2013). This ability or neutralising capacity is all dependent on the types and quantities present of neutralising material. Acid neutralising material needs to be rapidly available, however, the presence of such material does not guarantee prevention and neutralisation of leachate (Ahern, 2004, Devlopment, 2013). Additional factors that can influence and limit the ANC are surface coatings, such as iron oxides and gypsum through limiting surface area available for reactions. $CaCO_3$ is commonly used as a neutralising material as shown though* ***Equation 12*** *(Ahern, 2004),*

Equation 12: $CaCO_3 + 2H^+ + SO_4^{2-} + H_2O \rightarrow CaSO_4.2H_2O + CO_2$

As can be seen in the reaction of $CaCO_3$, one mole of calcium carbonate can effectively neutralise two moles of hydrogen ions, however not all the $CaCO_3$ proceeds to the completion of the reaction at near neutral pH (6.6-9.0) therefore a safety factor must be used of 1.5 to 2 to neutralise any acidity generated through AMD or from ASS (Ahern, 2004, Devlopment, 2013).

Dawesley Creek Water Parameters:

The baseline chemistry of Dawesley creek water that was used in the reactive modelling study is listed in **Table 9** below. This water is slightly alkaline with pH 8.1 and without appreciable quantities of trace metals and a low EC resulting in the water being defined as fresh water.

Table 9. Baseline chemistry for Dawesley creek, (Devlopment, 2013).

Parameter	Units	Dawesley Creek Water
pH		8.1
EC	µS/cm	1300
Acidity	mg/L $CaCO_3$	< 10
Acidity - calculated	mg/L $CaCO_3$	0
Alkalinity	mg/L $CaCO_3$	190
Residual alkalinity	mg/L $CaCO_3$	190
Ca	mg/L	37
K	mg/L	27
Mg	mg/L	26
Na	mg/L	190
Sulphate	mg/L	26
Al	mg/L	< 0.05
Cu	mg/L	0.009
Fe	mg/L	0.13
Mn	mg/L	0.004
Ni	mg/L	< 0.005

4.2 Data Analysis

4.2.1 Overview of data

The data collected throughout the column test work was a series of water analysis from both the supernatant water and leachate from the base of the column. A total of 14 samples were collected from the control Mix-0. A total of 15 samples were taken from all the other columns that were set up with various mixes of the co disposed material. As noted above in **Chapter 4.1.2**, there was two distinct Stages in the experiment, results from all columns consisted of 6 measurements from Stage 2b and 9 measurements from Stage 2a, the control column Mix-0 which had 8 measurements from Stage 2a as shown in **Figure 5** (Devlopment, 2013).

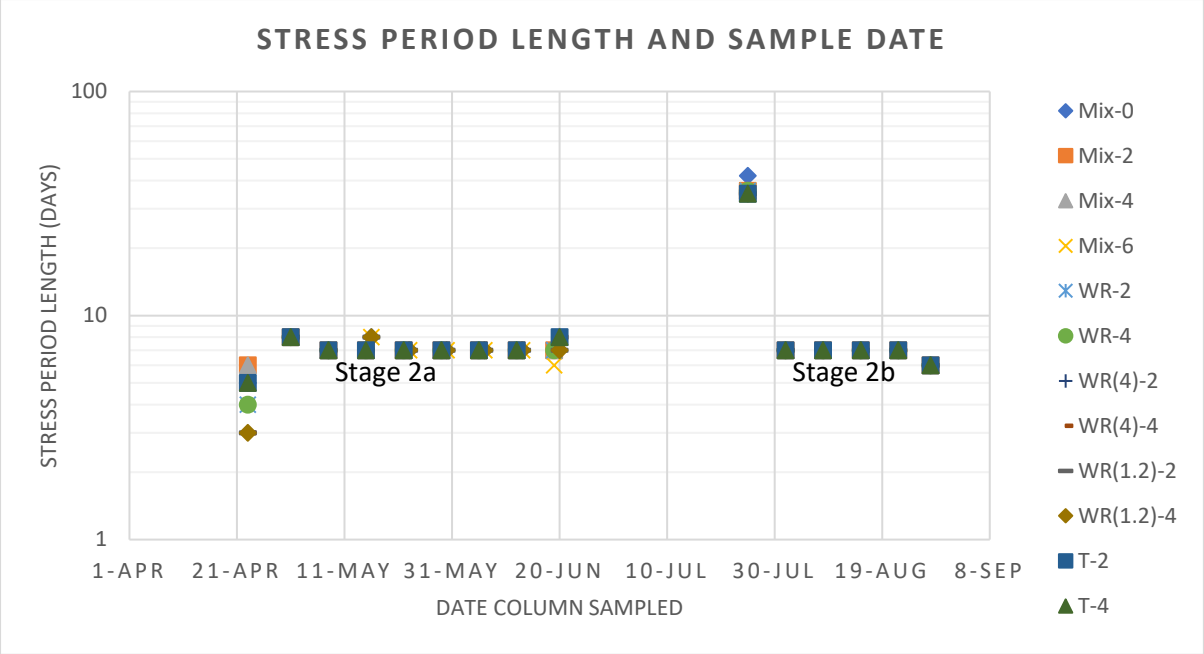

Figure 5. Graph showing the length of stress periods for each of the columns and the sampling date. Also showed is the distinction between Stage 2a and Stage 2b, along with the long intermission between the two different stages and a sampling event.

The following analytes Cl, As, Cd, Cr, F, Pb and Zn were all included in the Stage 2b analysis. Cl was not included in the Stage 2a analysis, however, given that Cl is a conservative ion and showed very little variation in Stage 2b (see **Table 10**), the concentrations of Cl were able to be estimated for Stage 2a based on the Stage 2b concentrations. This estimation was done using the first Cl concentration in Stage 2b.

Table 10. Comparison of the estimated chloride concentrations in Stage 2a to the measeured chloride concentrations of Stage 2b in 5 of the 12 column mixes. This is only for the leachate water that is produced.

Mix_0	**Stage 2a**	**312**	**312**	**312**	**312**	**312**	**312**	**312**	**312**	
	Stage 2b	312	302	334	308	304	322			
Mix_6A	Stage 2a	299	299	299	299	299	299	299	299	299
	Stage 2b	299	301	326	302	306	319			
WR_4	Stage 2a	310	310	310	310	310	310	310	310	310
	Stage 2b	310	308	320	309	307	335			
WR(1.2)_2	Stage 2a	312	312	312	312	312	312	312	312	312
	Stage 2b	312	308	324	311	322	316			
T4	Stage 2a	314	314	314	314	314	314	314	314	314
	Stage 2b	314	298	317	302	316	324			

The following analytes As, Cd, Cr, F, Pb and Zn are not able to be estimated in the same manner, been trace elements and non-conservative in nature. Concentrations of these elements showed limited variation in Stage 2b, with concentrations close to the laboratory limit of reporting for As, Cd, Cr, F and Pb throughout the duration of the experiment. Zn was an exception however, which showed notable variations in concentrations in Stage 2b from 8.65 mg/L at the start of the trial to

0.105 mg/L towards the end of the observation period in stage 2b, suggesting that elevated levels may have been present in Stage 2a.

Identifying the quality of data given for analysis is important and typically done though the ionic balance. This is calculated though **Equation 13** shown below. Hounslow (1995) states that if the ionic balance is equal to or less than 5%, then the analysis is assumed to be of adequate quality. However, if the ionic balance is greater than 5% then the analysis is potentially poor. Several factors may influence an ionic result greater than 5%. These factors include the exclusion of constituents which are present at elevated concentrations in the sample, organic ions may be present in large quantities, and/or the water may be very acidic (Hounslow, 1995).

Equation 13: $$Balance = \left(\frac{\sum C - \sum A}{\sum C + \sum A}\right) \times 100$$

It is noted that Stage 2a has very poor data quality having ionic imbalances of up to 80% in some measurements, see **Appendix A**. There is a discrepancy in data quality between the two laboratories, sulphate concentrations are three times greater at ALS compared to Eurofins | MGT, as shown in **Table 11**. Al and Ni are also observed as been three times greater when analysed at Eurofins | MGT compared to ALS. Applying a scaling factor of three to the sulphate concentrations generates more acceptable levels of ionic balance (see **Table 11**), however this does raise the issue of excessively high sulphate levels. The ionic balances in Stage 2b are considerably better, with most of the ionic balance of the analytes being below 10%. The only exception to this is in Mix-0 where the balance is 21.5% at its highest (see **Appendix A**).

Table 11. Data quality check of duplicate samples taken on May 8th, Stage 2a,from the two laboratories used, Eurofins | MGT and ALS. Stage 2a shows large irregularities in the data analysis, with ionic balance greater than 10%, with ALS concentrations of Sulfate observed as a third of Eurofins | MGT concentrations.

Parameter	Units	T-4 Leachate		WR(1.2)-4 Leachate	
		MGT	ALS	MGT	ALS
pH		6.4	6.45	6.5	6.3
EC	µS/cm	3700	3950	4700	4370
Acidity	mg/L $CaCO_3$	450	500	120	393
Acidity - calculated	mg/L $CaCO_3$	61	38	50	28
Alkalinity	mg/L $CaCO_3$	690	678	590	625
Residual alkalinity	mg/L $CaCO_3$	629	640	540	597
Ca	mg/L	790	736	670	666
K	mg/L	5.4	5	1	<1
Mg	mg/L	54	48	420	272
Na	mg/L	110	86	18	27
Sulphate	mg/L	460	1400	850	1740
Al	mg/L	0.46	<0.01	1.2	0.02
Cu	mg/L	0.014	0.007	0.056	0.014
Fe	mg/L	6.6	0.82	0.4	<0.05
Mn	mg/L	7.4	14.2	2.3	14.3
Ni	mg/L	16	5.75	22	1.16

4.2.2 Data Trends

There are a number of trends that can be observed across all the columns in the leachate trial conducted. Concentrations of Mg is observed as reducing across all of the columns, reducing to a concentration of 14mg/L (T-4) to 70 mg/L (WR(4)-4). Columns that contain just WR and finer material (WR(4)-2, WR(4)-4, WR(1.2)-2 and WR(1.2)- 4), had higher initial concentrations of Mg as shown in **Figure 6**. Columns that contained just the tailings material (T-2 and T-4), showed greatly reduced concentrations of Mg, with initial concentrations being 240 mg/L and 280 mg/L respectively, several orders of magnitude lower than all other column concentrations, reaching a final concertation of 14 mg/L and 15 mg/L for both T-2 and T-4 respectively (see **Figure 6**).

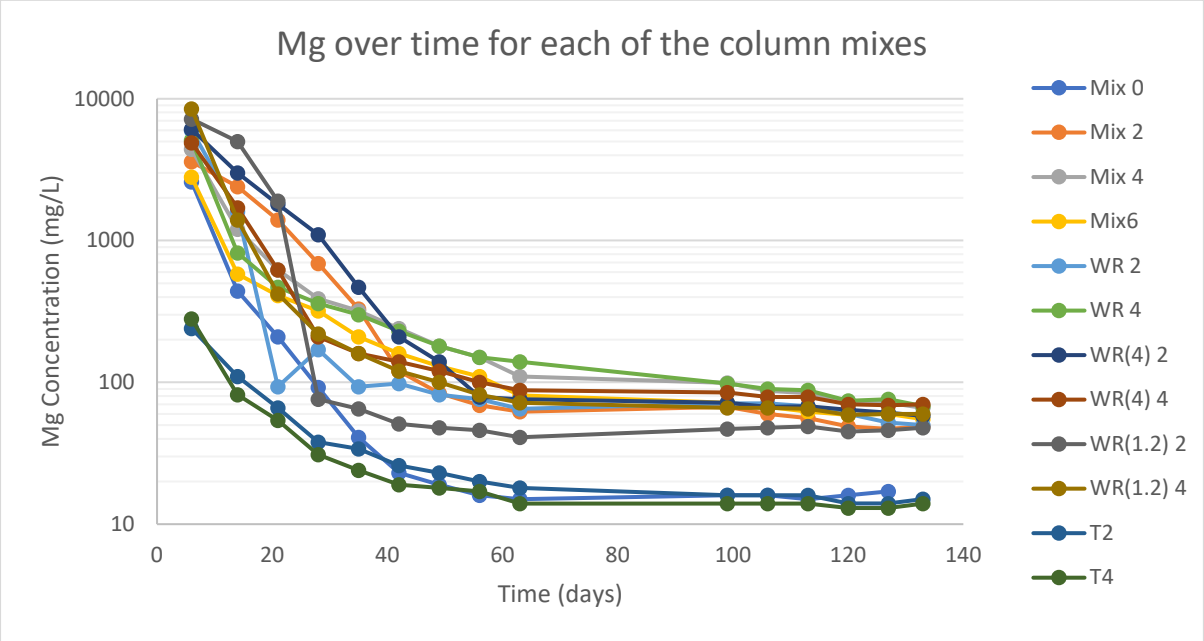

Figure 6. Mg concentrations over the time of the experiment expressed as days. Concentrations are done on logarithmic scale as concentrations start excessively high.

The pH increased with time across all the columns containing $CaCO_3$, increasing to a maximum of pH 6.97 in column T4 and a low of pH 6.27 in column WR(4)2 as shown in **Figure 7**. Increasing the amount of $CaCO_3$content in the column has minimal impact on the final pH, as observed in Mix2 and Mix 6 which both resulted in pH 6.52. Columns containing 4% wt. of $CaCO_3$ resulted in the final pH being 0.2-0.3 higher than columns that contained 2% wt. of $CaCO_3$. However, the initial pH of the column at the beginning of the leachate trials starts considerably higher with 6% wt. of $CaCO_3$, at pH 5.8, compared to columns with 2% and 4% wt. of $CaCO_3$, maximum of pH 4.6 (WR4) (see **Figure 7**).

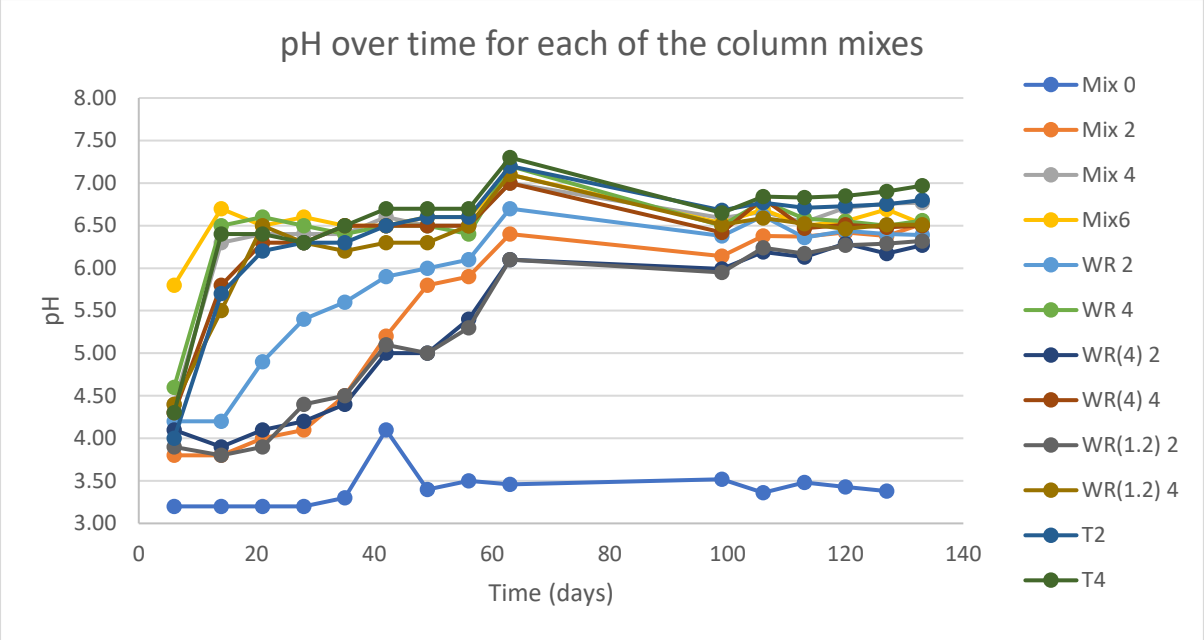

Figure 7. pH of the columns over the course of the column experiment.

The Ca^{2+} concentrations tend to follow the same type of increase as the pH increases in the columns. In the mix columns mix 2 is shown as having a slower increase in pH over time which coincides with the Ca2+ increase over the same period. This same Ca2+ slow increase is also noted in WR(1.2)2 and WR(4)4 which also have a slower increase in pH (see figure XX). In contrast columns that have a sharp increase in pH also have a sharp increase in C12+.

Sodium (Na^{+}) concentrations are shown to be increasing across all columns to a concentration between 192 mg/L in Mix-0 to 292 mg/L in column WR(1.2)-4 which can be observed in **Figure 8**. As there is increases in Na+ occurring across all columns indicates that there is mineral dissolution which involves Na^{+}, as the Dawesley creek water has a lower overall concentration of Na^{+} compared to the final concentration observed in the leachate of some columns, as seen in **Table 9**.

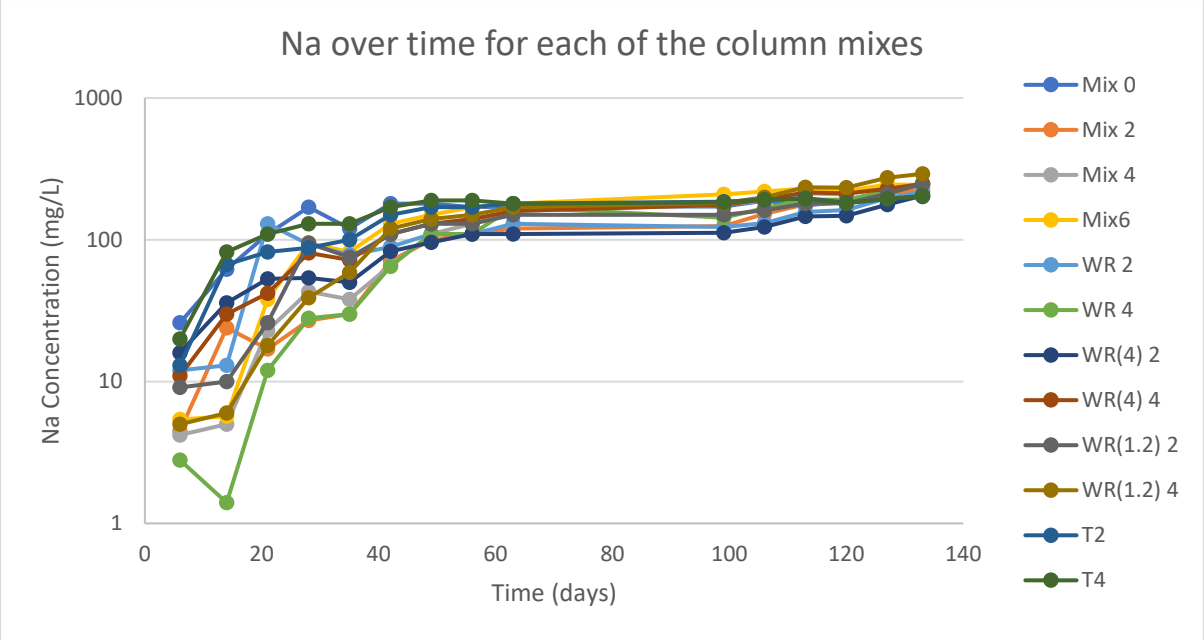

Figure 8. Na concentrations of the columns over the course of the column experiment.

Concentrations of Fe are observed as decreasing across all columns with $CaCO_3$ present by three orders of magnitude (see **Figure 9**). The initial concentrations for Fe are also shown to be affected by the amount of $CaCO_3$ present in the column. Columns with only WR or tailings are observed as having a magnitude of difference between the 2% wt. and 4% wt. of $CaCO_3$. Finer sediment columns just show this trend for material <1.2mm. material with <4mm had concentrations of Fe that were extremely similar (WR(4)2 Fe 19mg/L, WR(4)4 Fe 21mg/L) (see **Figure 9**). At near neutral pH Fe may be sorbed to other minerals, the same could be said for Al concentrations across all the columns with CaCO3 present as shown in **Figure 10**. Like Fe, at near neutral pH Al may be sorbed onto other minerals, while remain in solution in acidic conditions. There is a clear relationship and trend that is shown in figures XX and XX between pH, Fe and Al.

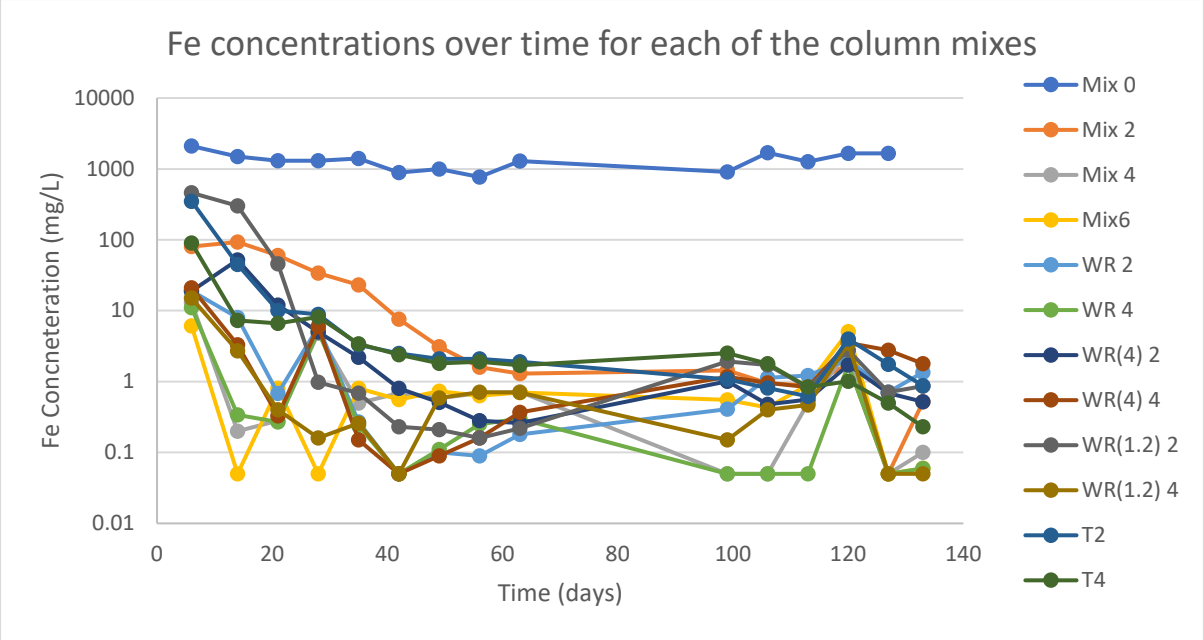

Figure 9. Fe concentrations of the columns over the course of the column experiment. Concentrations are done on logarithmic scale as concentrations start excessively high.

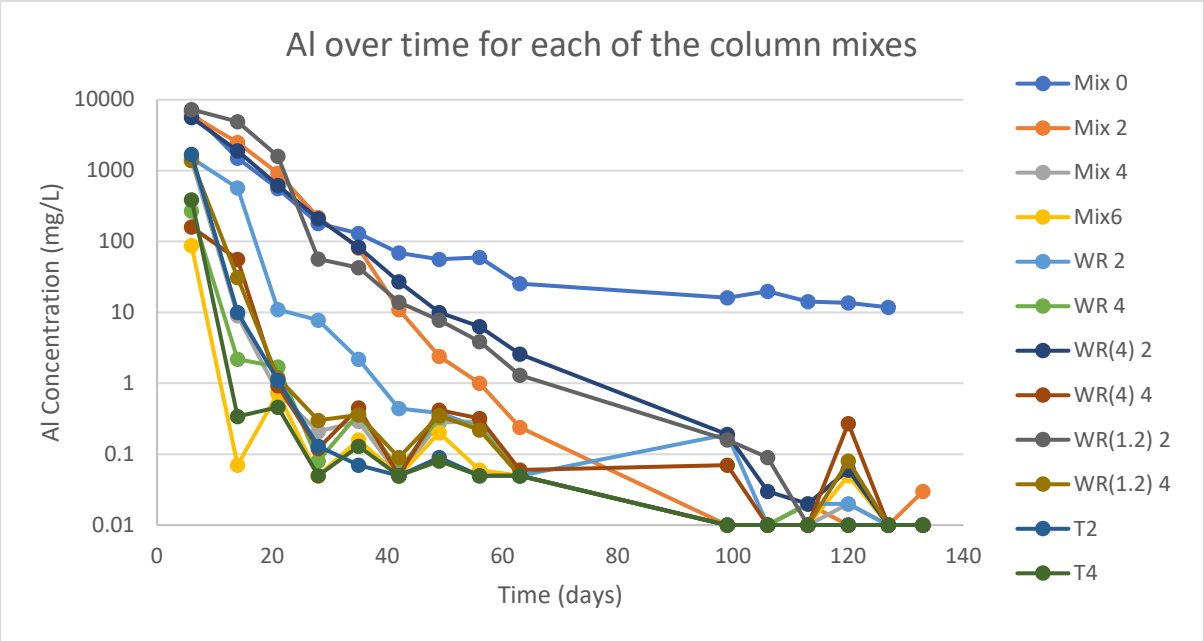

Figure 10. Al concentrations of the columns over the course of the column experiment. Concentrations are done on logarithmic scale as concentrations start excessively high.

4.2.3 Identification of mineral in columns

Primary minerals that are assumed to be responsible for the key reactions require identification in each of the columns. The four assumed key minerals are Gypsum, $CaCO_3$, Jarosite and FeS_2. All minerals identified need to be converted from %wt. to mol/L for input into the reactive transport model, this was done using **Equation 14** below.

Equation 144: $$\frac{mol}{L} = \frac{(wt.of\ element\ in\ 1g\ of\ soil \times density\ of\ soil)}{molecular\ wt.of\ element}$$

Concentrations of $CaCO_3$ is reported in each column as wt.% ANC. Columns contain a mixture of both WR and tailings, both of which require the identification of Other minerals that may be present in the portion of WR and tailings in each column. As stated above gypsum is reported as S_{KCl}, FeS_2 is S_{TOS} and Jarosite is S_{NAS}, with FeS_2 and jarosite being identified though **Equations 9** and **Equation 8**. The results for each column are shown below in **Table 12**,

Table 12. Column compostion for each of the columns, showing pertage of waste rock, tailings and CaCO3 and mol/L of CaCO3, Pyrite, Jarosite and Gypsum. Note WR(1.2)-2 has no CaCO3 measurement recorded in data provided, but is assumed to be 2%wt..

Column Name	%Wt. of CaCO3	% of Tailings	% of waste rock	CaCO3 mol/L	Pyrite mol/L	Jarosite mol/L	Gypsum mol/L
Mix-0	0.02%	37.00%	63.00%	0.00313	0.5999	0.1722	0.1106
Mix-2	2.54%	36.00%	62.00%	0.4085	0.6036	0.1737	0.1114
Mix-4	4.86%	36.00%	60.00%	0.7987	0.6034	0.1724	0.1108
Mix-6A	5.87%	35.00%	59.00%	0.6650	0.4074	0.1167	0.1041
WR-2	2.00%	0.00%	98.00%	0.3235	0.6433	0.2474	0.0749
WR-4	4.46%	0.00%	96.00%	0.7161	0.6255	0.2405	0.1484
WR(4)-2	3.05%	0.00%	98.00%	0.4723	0.6159	0.2369	0.1443
WR(4)-4	4.60%	0.00%	96.00%	0.7022	0.5948	0.2287	0.1421
WR(1.2)-2	-	0.00%	98.00%	-	0.6135	0.2359	0.1372
WR(1.2)-4	4.00%	0.00%	96.00%	0.5783	0.5632	0.2166	0.1415
T-2	1.57%	98.00%	0.00%	0.2233	0.4788	0.0435	0.1299
T-4	4.45%	96.00%	0.00%	0.6504	0.4818	0.0438	0.0435

Chapter 5 Reactive transport Model setup

5.1 Conceptual model

When designing a groundwater model, it is common to start simple and build up complexity, however, oversimplification during the conceptual stage cannot always be corrected which may lead to an inaccurate model, or if there is a lack of data to assist in constraining the model (Jasna et al., 2004). The conceptual stage of this model is separated into two different elements , the flow model and the reactive transport model. The flow model is kept simple and based on the design of the saturated column of sediments as outlined in **Chapter 4.1.3**. The reactive transport model is more complicated, as the complete composition of the material is not known. However, the reactive transport model is also kept relativity simple through including the known minerals present in the co-disposed material, including the kinetics of FeS_2 as a driving reaction. MODFLOW was the modelling programme used to build the groundwater flow model. The reactive transport model was implemented through PHT3D which combines MODFLOW and PHREEQC in order to simulate the reactions and geochemistry of the leachate. Each of element of the modelling process is discussed in the following sections below.

5.2 Flow Model

A two-dimensional model of the columns was defined to simulate the column experiments. This consisted of one row and column, with an easting and northing of 0.16838 m, giving the same cross-sectional area as a diameter of 19 cm of the columns used in the experiment. The vertical extent of the model was separated into 26 layers, which were used to represent the 50 cm depth of co-disposed material, this resulted in a vertical discretisation of 1.923 cm per layer. Vertical discretisation of this size will allow for adequate simulation to obtain results accurate enough to define reaction that are taking place in a timely and efficient manner. As this is a transient model, the time period was set to days, with 28 stress periods. Stress periods were split into no flow, where the column was left to stand, and flow periods, where the leachate was left to drain out during sampling events. The total volume drained from the column model created was based on the sampling volumes obtained during each sampling event in the column leachate test. These stress periods varied in length to represent the sampling periods and standing times of the columns (see **Figure 5**). Finer discretization of the time steps and period length was used during flow periods to reduce numerical errors (Delleur, 2006). To simulate the refilling/topping up of the columns during the flow periods a constant head cell was established at the top of the column. This constant head cell maintained a constant flux of water entering the model at the top of the model, as shown in **Figure 4**. The chemical composition of this water was the same as Dawesley creek water, as mentioned earlier in **Chapter 4.1.3**.

As only approximate durations were recorded for each sampling event (30minutes to 4hours), the model was set-up with an average two hours sampling period during each flow period. This was kept constant across all the columns. A constant hydraulic conductivity of 1.783 m/day was also kept constant across all columns modelled. This hydraulic conductivity was considered adequate from the description of the materials used and from a range of hydraulic conductivities as shown in **Table 13**. The co-disposed material used had a grain size of <25mm (Devlopment, 2013), considered medium/fine gravel with course sand (Fetter, 2014). A range of hydraulic conductivities for medium/fine gravel with course sand or well graded course sand can be seen in **Table 13**.

Table 13. Range of hydraulic conductivities for medium/fine gravel with course sand or well graded course sand from various sources.

Source	Hydraulic Conductivity
Appelo and Postma (Appelo and Postma, 2005)	10-300 m/day
Fetter (Fetter, 2014)	0.756-7.560 m/day
Freeze and Cherry (Fetter, 2014)	0.756-7.560 m/day

The hydraulic conductivity of 1.783 m/day was used for both vertical and horizontal conductivities. The porosity of the columns was calculated using **Equation 15**, the porosity for each of the columns can be seen in **Table 14**. Gradients were altered to match the volume of leachate collected during periods of no flow and flow (as seen in **Figure 5**). This was calculated using Darcy's Law, rearranged as shown in **Equation 16** (Ahern, 2004, Fetter, 2014, Freeze and Cherry, 1979).

Table 14. Porosity of each column expressed as a percentage. Volume of voids and the total volume are also displayed.

Column Name	Volume of Voids (L)	Total Volume (L)	Porosity (%)

Mix-0	5.46	14.176	38.51580135
Mix-2	5.22	14.176	36.8227991
Mix-4	5.03	14.176	35.48250564
Mix-6A	7.87	14.176	55.51636569
WR-2	5.18	14.176	36.54063205
WR(4)-2	5.24	14.176	36.96388262
WR(1.2)-2	5.56	14.176	39.22121896
WR-4	5.68	14.176	40.06772009
WR(4)-4	3.74	14.176	26.38261851
WR(1.2)-4	6.13	14.176	43.24209932
T-2	6.26	14.176	44.15914221
T-4	6.04	14.176	42.60722348

Equation 15: $n = \frac{100 \cdot V_v}{V_T}$

where,

n *is porosity expressed as a percentage*

V_v *is volume of the voids*

V_T *is total volume*

An initial head height of 0.5 m, as shown in **Equation 16**, was used as this is the total height of the sediment, from which the gradient was then calculated. The calculated gradient during stress periods of flow for each of the columns can be seen in **Appendix B**. This was put into the model though MODFLOW's time variant head allowing for the appropriate gradient to obtain the same amount of leachate during the column leachate experiment.

Equation 166: $Q = -KA\frac{dh}{dl}\ \ rearragenged\ as, \frac{dh}{dl} = 0.5 - \frac{Q}{KA}$

Where,

Q *is the Darcy flux/velocity*

K *is the hydraulic conductivity of the material*

A *is the cross-sectional area*

$\frac{dh}{dl}$ *is the gradient*

5.3 Geochemical transport model

Geochemical transport model was established though PHT3D, which builds on the flow model though hydrogeochemical reactions and mineral kinetics. For this model there was five minerals that were considered key, as these minerals are considered to consist the bulk of the material. The reactions from these minerals alter the chemistry of the water in the saturated material, affecting the leachate, the key minerals were $CaCO_3$ (**Equation 17**), Dolomite (**Equation 18**), Gypsum

(**Equation 19**), Jarosite (**Equation 10**) and FeS_2 (**Equation 20**), each of these minerals had important dissolution reactions as shown below.

Equation 177. $CaCO_3 + H^+ \leftrightarrow Ca^{2+} + HCO_3^-$

Equation 188. $CaMg(CO_3)_2 + 4H^+ \leftrightarrow Ca^{2+} + Mg^{2+} + CO_3^{2-} + 2H^+$

Equation 19. $CaSO_4 \cdot 2H_2O \leftrightarrow Ca^{2+} + SO_4^{2-} + 2H_2$

Equation 20: $FeS_2 + 2H^+ + 2e^- \rightarrow Fe^{2+} + 2HS^-$

Each of the minerals stated are put into the model in concentration as $\frac{mol}{L} bulk\ aquifer\ vol.$ as identified in **Chapter 4.2.3**. Although these minerals, FeS_2, Jarosite, $CaCO_3$, Gypsum and Dolomite are the primary minerals of interest in the reactions, there are several other minerals considered as secondary reactions. As Fe^{3+} is oxidised this precipitates out as $Fe(OH)_3$, releasing up to three quarter of the acidity generated in the overall reaction of FeS_2 oxidation (**see Figure 1**), however this reaction is highly pH dependant (Appelo and Postma, 2005). Goethite may release Fe^{3+} resulting in similar reactions as with the oxidation of FeS_2 and the reduction of the overall pH, while siderite my assist in maintaining the pH or raising the pH through the reaction shown in **Equation 21**.

Equation 19: $FeCO3 \rightarrow Fe^{2+} + CO_3^{2-}$

These minerals were added to the model, however as concentrations for these minerals is unknow, they were amended to equilibrate with the modelled data.

When setting up the hydrogeochemical model the number of components needs to be considered, the elements / components for this model can be seen in the **Table 15** below. This includes the minerals mentioned above as minerals in equilibrium. The unknown concentrations of minerals were altered to equilibrate to the saturation index of the mineral, governing the rate of dissolution into the solution or precipitation from the solution accordingly.

Table 15: Components included in model and if the concentration is known or unknown for each

Element/component	Concentration
$\boldsymbol{pH}$	Known for each column and creek water
$\boldsymbol{Ca^{2+}}$	Known for each column and creek water
$\boldsymbol{Cl^-}$	Known for each column and creek water
$\boldsymbol{Fe}$	Known for each column and creek water
$\boldsymbol{K}$	Known for each column and creek water
$\boldsymbol{Mg^{2+}}$	Known for each column and creek water
$\boldsymbol{Na}$	Known for each column and creek water
$\boldsymbol{O}$	Known for each column and creek water
$\boldsymbol{S}$	Known for each column and creek water
Mineral/component	**Concentration**
Pyrite	Known for each column
Jarosite	Known for each column
Calcite	Known for each column
Gypsum	Known for each column
Dolomite	Known for each column
Siderite	Unknow

Goethite	Unknow
Haematite	Unknow

FeS_2 dissolution or precipitation was considered as a kinetic reaction based on the established reaction rate by Williamson and Rimstedt (Appelo and Postma, 2005) , see **Equation 4-6**. The initial concentration of the element/components mentioned in **Table 15** are the same as Dawesley creek water as this is what was used to irrigate the columns, while the initial concentration of the minerals identified are from the static geochemical test conducted on the material used in the columns. The initial D.O was set at atmospheric concentrations to begin with throughout the entire column. This was done as the material was exposed to atmospheric oxygen during the initial setup of the column experiment.

Chapter 6 Results from model

The results are split into three different section that are focused around the three different simulations that were run for each of the 12 columns. The first simulation was run using the default dispersion with a molecular dispersivity coefficient of zero. The second simulation was runs using a calculated molecular dispersivity coefficient of $8.64 \times 10^{-5} m/day$. The final simulation built upon the second simulation through adding the minerals goethite and haematite.

The first section of the results is focused on these three different simulations in the mixes of WR and tailings blended with the various amount of $CaCO_3$. The second section of the results is focused on the three different simulations in the WR and various amounts of limestone. The final section of the results is focused around the two columns that were based on just tailings material with limestone looking at the three different simulations. In all the simulations, particular features that are considered integral in identifying the evolution of the hydrogeochemical processes taking place, are outlined. These are pH, SO_4^{2-}, total Fe, FeS_2 and $CaCO_3$. Each is detailed in what was observed from the results of each of the three simulations for each column. In each of the figure presented in the following section 'Obs 1' is the simulated concentration at the top of the simulated column, 'Obs 2' is the simulated concentration in the middle of the column and 'Obs 3' is the simulated concentration at the base of the column, the green dots shown are the observed results from the column experiment that are attempted to be simulated.

6.1 Waste Rock and Tailings Mixes

6.1.1 pH

The initial simulation of Mix-0 the modelled pH started higher than the observed pH of 3.2, this then dropped to pH 3.25 where it was maintained at the base of the column as shown in **Figure 11**. It is also observed in **Figure 11** that the middle of the column has a similar profile to the base of the column, though reduces earlier at 20 days. While the base starts to reduce at 30 days. The top of the column reduces to a pH 3.6, then rebounds during the draining and refilling periods. This is observed to happen continuously throughout the simulation as seen in **Figure 11**. At the intermission between stage 2a and stage 2b all three observations points, top middle and base, the pH is reduced pH 3.25. However, for the top observation this rebounds back to a pH 5.4 once sampling resumes. In the second simulation of Mix-0 the simulated results observed at the base started at pH 5.5 and started dropping and rising during sampling and refilling, reaching a low of pH 3.75 during stage 2a (seen **Figure 12**). The simulated pH observation in the middle of the column was not being reduced as

severely as the base. However, during the intermission between Stage 2a and Stage 2b the pH at all three observations was reduced to pH 3.25, as can be seen in **Figure 12**. Though this low pH did rebound quickly during draining and refilling at the middle and top observation points. The pH at the base remained low, which was like the observed levels in the column experiment as seen in **Figure 12**. In the final run for Mix-0 the simulated pH starts extremely low at 1.0 for all the observation points, top middle and base, as observed in **Figure 13**. At the top observation the pH rises quickly to pH 6.5 at 30 days where it is maintained between pH 6.5 and pH 7.5. In Stage 2a the pH at the base rises in a step wise fashion till 50 days (see **Figure 13**), where the pH is similar to the observed pH in the column experiment. In in Stage 2b the simulated pH at the base is like the observed pH from the column experiment.

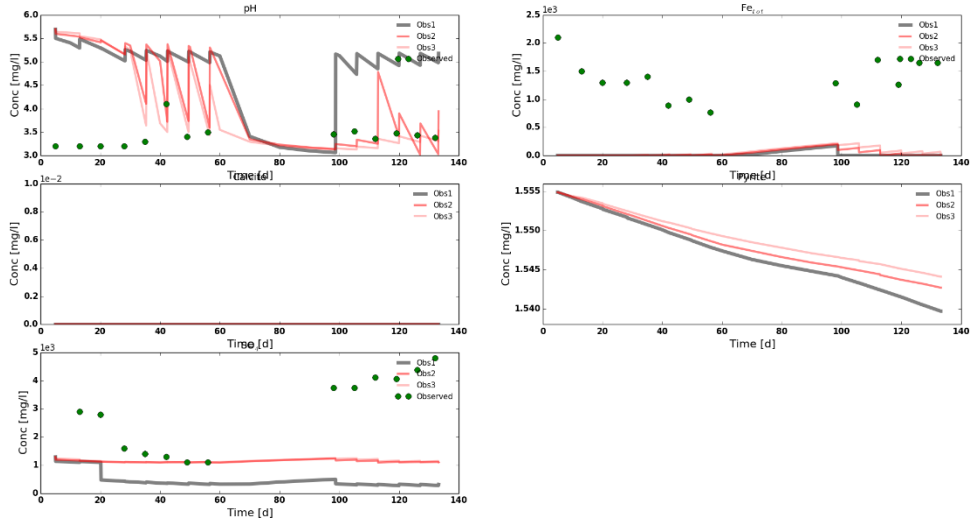

Figure 11. Simulated results from the initial run of Mix-0 showing concertation over time for pH (top left), total Fe (top right), Calcite (middle left), pyrite (middle right) and sulphate (bottom left). Green dot are the observed results from the column experiments conducted.

Mix-2 and Mix-4 are similar in the pH profiles that were developed during the initial simulation. The pH is at a consistent level with little variation at pH 6.0 for both the base and the middle of the column as shown in **Figure 14** and **Figure 17**. The observation at the top of the column starts at pH 6.0 then start to rise slowly in a step wise fashion from 20 days through to the end of Stage 2a (see **Figure 14** and **Figure 17**). This rise in pH at the top of the column reaches a peak of pH 6.5 during Stage 2a. At the beginning of Stage 2b the top observation pH was reduced to pH 6.2, however this begins to rise again in a similar profile as Stage 2a, reaching a peak pH 6.75 as shown in **Figure 14** and **Figure 17**. The second simulations of Mix-2 and Mix-4 had extremely similar profiles to the initial run (see **Figures 14, 15, 17 and 18**). In the final simulation of Mix-2 the pH starts higher than the observed from the column experiment, at pH 5.5 for all three of the observation points. All three observation points rise in a step wise fashion with the base and middle reaching pH 6.75 before the intermission between Stage 2a and Stage 2b (see **Figure 16**). During Stage 2b the simulated pH at the base is very similar to the observed pH from the column experiment as shown in **Figure 16**. The final simulation of Mix-4 is like Mix-2, however the simulated pH is very close to the observed pH in Stage 2a as well as Stage 2b as shown in **Figure 16** and **Figure 19**.

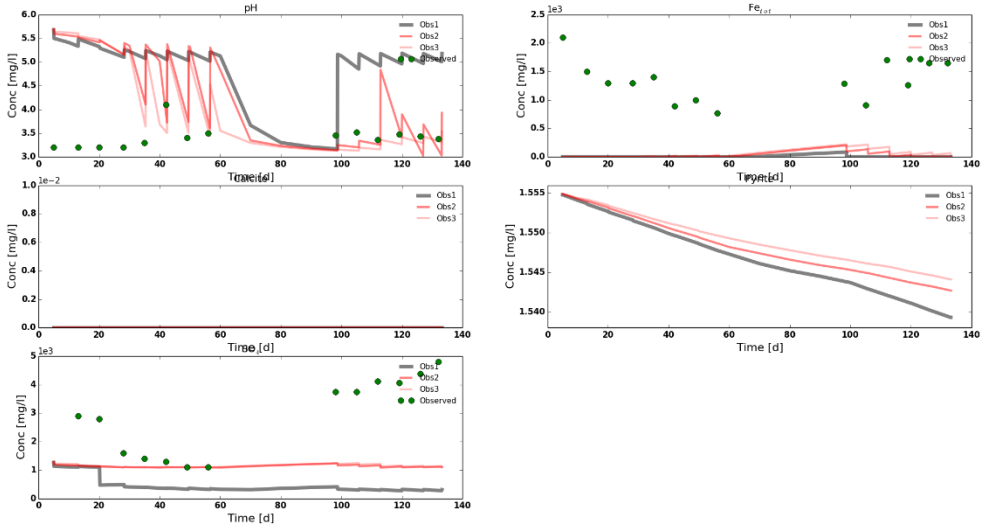

Figure 12. Simulated results from the second simulation of Mix-0 showing concertation over time for pH (top left), total Fe (top right), Calcite (middle left), pyrite (middle right) and sulphate (bottom left). Green dot are the observed results from the column experiments conducted.

The pH in the initial simulation of Mix-6 shows the simulated results in the middle and base of the column start at pH 6.0 and maintain this for the entire simulation, as shown in **Figure 20**. The top observation rises in a step wise fashion like Mix-2 and Mix-4, however this rise started immediately and reached a peak of pH 6.8 at the end of Stage 2a (see **Figure 20**). In Stage 2b the pH at the top of the simulated column of Mix-6 reached a peak of pH 6.9. The second simulation of Mix-6 was like the initial simulation, however the pH rise at the top observation of the column is more pronounced rising from pH 6.0 to pH 7.0 in Stage 2a and to a peak of pH 7.3 in Stage 2b. There is also a rise of the pH in the middle of the column, see **Figure 21**, starting at 30 days reaching a maximum of pH 6.2. The base observation saw a rise in the simulated pH in Stage 2b to pH 6.6, see **Figure 21**, in a step wise fashion, getting closer to the observed pH from the column experiment. In the final simulation Mix-6 starts with a slightly higher pH than Mix-2 and Mix-4 but has a similar profile, see **Figure 22**. There is a period in Stage 2a, at 35 days to 55 days where the simulated pH is like the observed pH from the column experiments. In Stage 2b of Mix-6 the simulated pH is like the observed pH for four of the six observations simulated (see **Figure 22**).

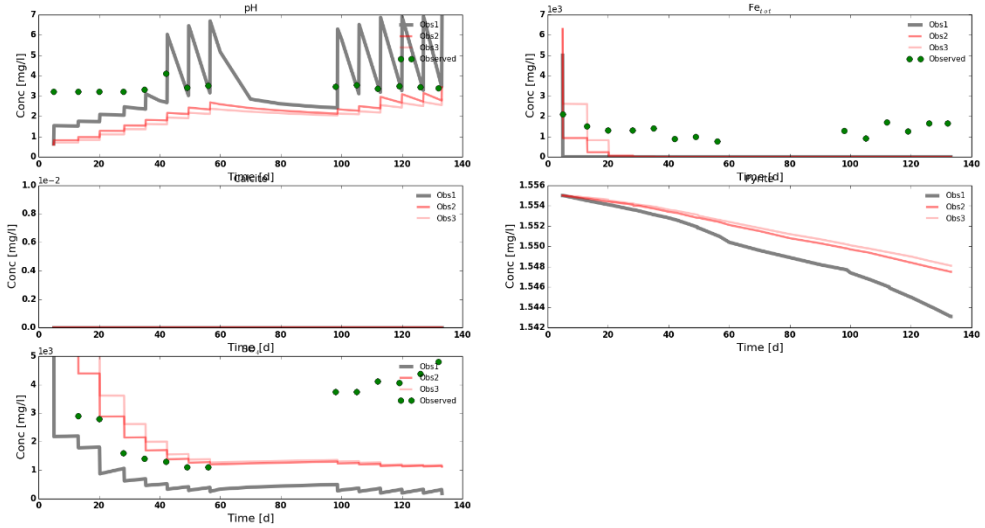

Figure 13. Simulated results from the final simulation of Mix-0 showing concertation over time for pH (top left), total Fe (top right), Calcite (middle left), pyrite (middle right) and sulphate (bottom left). Green dot are the observed results from the column experiments conducted.

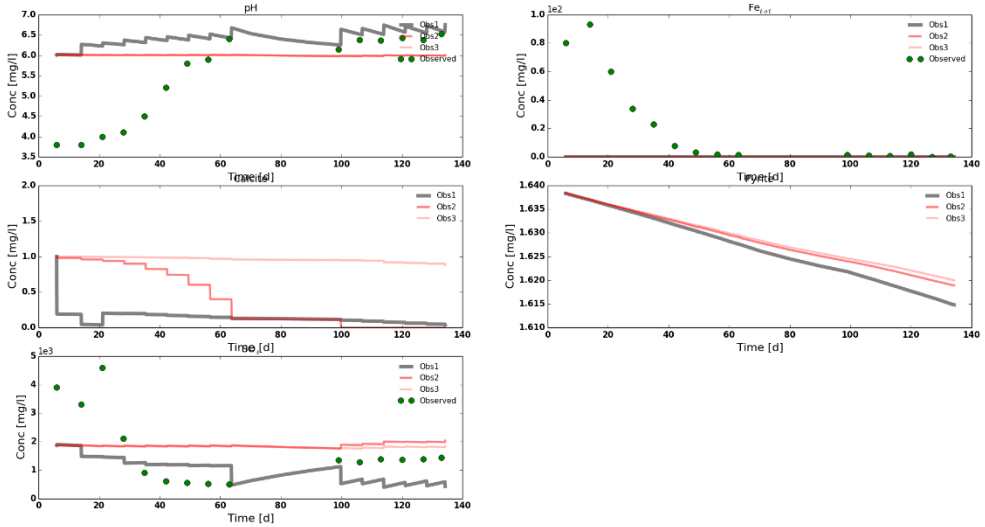

Figure 14. Simulated results from the initial simulation of Mix-2 showing concertation over time for pH (top left), total Fe (top right), Calcite (middle left), pyrite (middle right) and sulphate (bottom left). Green dot are the observed results from the column experiments conducted.

6.1.2 SO_4^{2-}

In the initial simulation the sulphate in Mix-0 started with a relatively low concentration in comparison to the observed concentrations, at around 1300mg/L, as shown in **Figure 11**. Though Mix-2, Mix-4 and Mix-6 all started with an initial simulated concentration of around 2000mg/L (as shown in **Figures 14, 17 and 20** respectively). However, throughout the simulation of each column, Mix-0 was the only column that had a rise in the sulphate concentrations at the base observation point. The other columns maintained a constant concentration throughout (see **Figures 14, 17 and**

20). Mix-2, Mix-4 and Mix-6 all had simulated results close to observed in Stage 2b while Mix-0 only had a few sampling periods in Stage 2a that were similar to the observed concentrations. The sulphate concentrations at the top observation where similar in Mix-2 and Mix-4. The middle observation in all the simulated columns was the same as the base observation. In the second run Mix-0 is very similar to the initial run with a slight rise in sulphate concentration at the base getting to 1500mg/L (see **Figure 12**). As observed in **Figure 15** and **Figure 18**, Mix-2 and Mix-4 showed the same results in the simulation, having a slight increase in concentration at the base, increasing slightly over 2000mg/L. Giving simulated results similar to the observed results in Stage 2b. Mix-6 did not display a drop in sulphate levels at the base of the simulated column until 100 days, Stage 2b, which gives simulated results like the observed results (see **Figure 21**). In the final simulation of Mix-0 the simulated results show that the sulphate started in excess of 5000mg/L.

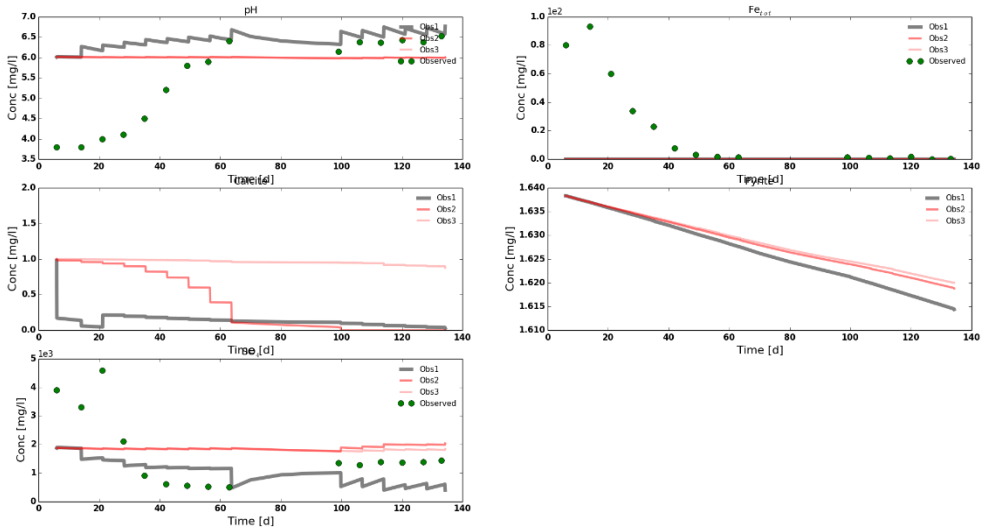

Figure 15. Simulated results from the second simulation of Mix-2 showing concertation over time for pH (top left), total Fe (top right), Calcite (middle left), pyrite (middle right) and sulphate (bottom left). Green dot are the observed results from the column experiments conducted.

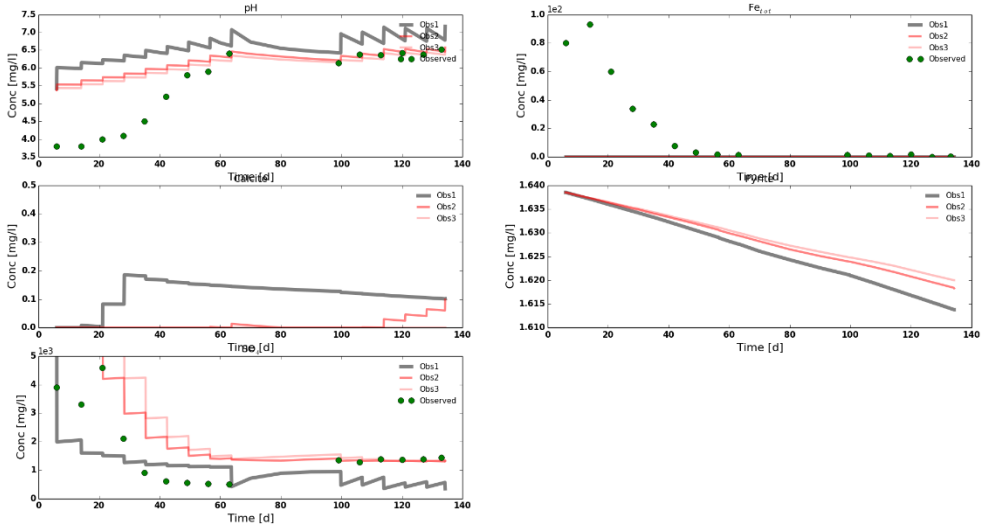

Figure 16. Simulated results from the final simulation of Mix-2 showing concertation over time for pH (top left), total Fe (top right), Calcite (middle left), pyrite (middle right) and sulphate (bottom left). Green dot are the observed results from the column experiments conducted.

Though this high concertation drops throughout stage 2a, with the simulated concentrations matching up with the observed results (see **Figure 13**). However, Stage 2b the simulated concentrations remain low at around 1200mg/L. The final simulation of Mix-4 is like Mix-0 as observed in **Figures 19 and 13** respectively, however the simulated results show the same trend as the observed concentrations. However, this is at a magnitude higher than the observed as seen in **Figure 19**. The final simulation of Mix-2 starts with excessive concentrations of sulphate as well, though this declines from 20 days and continues until 50 days where it stabilises at a concentration of 1300mg/L for the remainder of the simulation (see **Figure 16**). The final simulation of Mix-6 starts with a concentration greater than 5000mg/L, though this drops to 3000mg/L at 15 days. This decline continues at a slower rate until 35 days, as seen in **Figure 22**, where the simulated concentration stabilises at 1400mg/L. Stage 2b shows observed and simulated results that are very close as seen in **Figure 22**, while stage 2a the observe results remain below 1000mg/L.

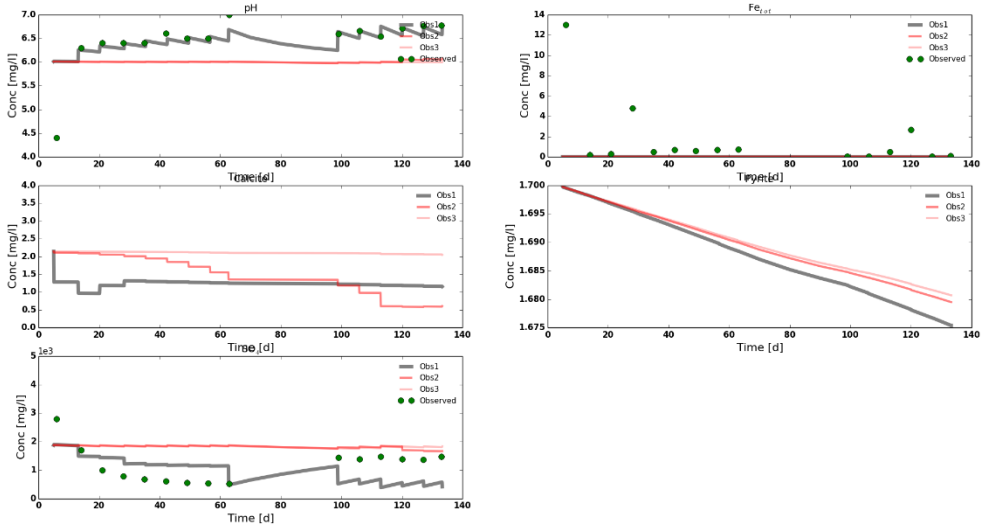

Figure 17. Simulated results from the initial simulation of Mix-4 showing concertation over time for pH (top left), total Fe (top right), Calcite (middle left), pyrite (middle right) and sulphate (bottom left). Green dot are the observed results from the column experiments conducted.

6.1.3 Total Fe

Mix-0 starts with an initial simulated concentration that is at trace concentrations <0.0mg/L. However, this begins to rise throughout the simulation, as seen in **Figure 11**, particularly during the intermission between Stage 2a and Stage 2b. The concentration at the base of the column reaches a peak of 500mg/L in Stage 2b. Though this is excessively low compared to what was observed during the column experiment as seen in **Figure 11**. Mix-2, Mix-4 and Mix-6 all had extremely low concentrations of total iron throughout the initial simulation, as seen in **Figures 14, 17 and 20** respectively, compared to the observed results. These simulated columns maintained a trace concentration <0.0mg/L, this was also observed in the second and final simulations for these mixes. The second simulation of Mix-0 had no significant change in the concentration, starting at <0.0mg/L and maintain this throughout Stage 2a. During the intermission between Stage 2a and Stage 2b, there was a rise in concentration (see **Figure 12**). This reached a peak of around 200mg/L. However, this quickly diminishes after Stage 2b sampling began. In the final run the total iron in Mix-0 starts rather high at around 6400mg/L, however this is quickly flushed out as shown in **Figure 13**. At 15 days the simulated concentration of Fe in Mix-0 is less than 1000mg/L, and after 20 days it is at <0.0mg/L and remains at this level for the remainder of the simulation.

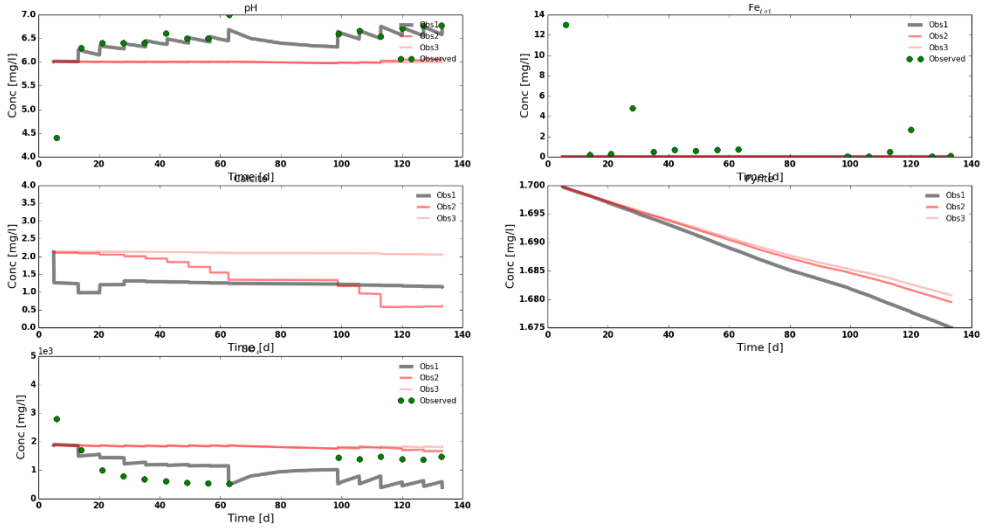

Figure 18. Simulated results from the second simulation of Mix-4 showing concertation over time for pH (top left), total Fe (top right), Calcite (middle left), pyrite (middle right) and sulphate (bottom left). Green dot are the observed results from the column experiments conducted.

6.1.4 FeS_2

The FeS_2 dissolution in the initial simulation is shown to be occurring throughout the entire column, at all three observation points. At the base observation in Mix-0, less than 1% of the wt.% in the column is been dissolved throughout both Stage 2a and Stage 2b, as seen in **Figure 11**. in the second simulation, the dissolution of FeS_2 has less variation at the base, middle and top of the column (see **Figure 12**). However, it is still less than 1% of the wt.% of the FeS_2 concentration that is been dissolved. In the final run the base and middle concentrations of FeS_2 are similar to each other, though the top observation seems to have a greater dissolution of FeS_2 throughout the column experiment.

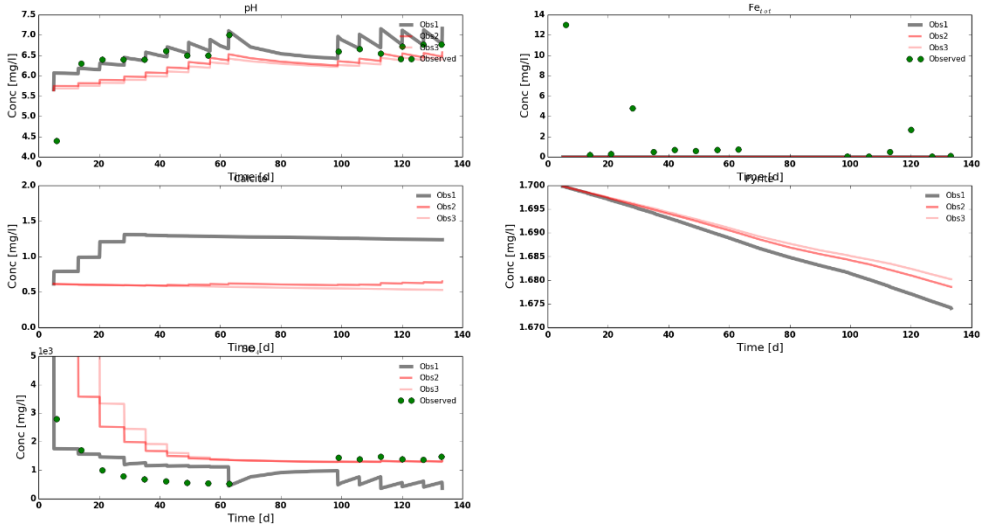

Figure 19. Simulated results from the final simulation of Mix-4 showing concertation over time for pH (top left), total Fe (top right), Calcite (middle left), pyrite (middle right) and sulphate (bottom left). Green dot are the observed results from the column experiments conducted.

All three simulations of Mix-2, Mix-4 and Mix-6, all show dissolution of FeS_2 greater than 1% but less than 2% of the wt.% of the column. It is also noted that Mix-2, Mix-4 and Mix-6 all show similar profiles for dissolution of FeS_2 at the top middle and base in the second and final run (see **Figures 15, 16, 18, 19, 21 and 22**). The initial run still presents a larger variation in concentration across all Mixes and all three observation points.

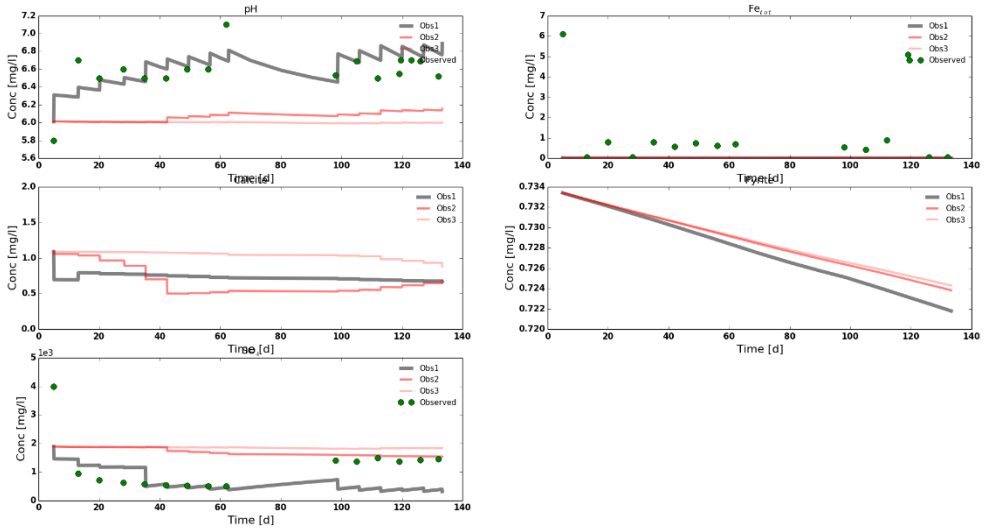

Figure 20. Simulated results from the initial simulation of Mix-6 showing concertation over time for pH (top left), total Fe (top right), Calcite (middle left), pyrite (middle right) and sulphate (bottom left). Green dot are the observed results from the column experiments conducted.

6.1.5 $CaCO_3$

For Mix-2 the initial and second simulation of the column started with a concentration of 1.0mg/L at all three observation points. The base was maintained at 1.0mg/L for the duration of the of the simulation. The middle observation showed a slow decline to begin with, which steadily increased reducing the concentration from 1.0 to 0.2mg/L by the end of Stage 2a (see **Figure 14** and **Figure 15**). The remainder of the simulation there was a slight decrease to a concentration of 0.0mg/L. The top observation had a sharp decline initially to 0.2mg/L, where it continued to decline over the remainder of the simulation. In the final simulation of Mix-2, which can be seen in **Figure 15**, the base was observed at keeping a concentration of around <0.0mg/L for the duration of the simulation. The middle observations start at <0.0mg/L, however has a slight increase at the beginning of the intermission between Stage 2a and Stage 2b. Another increase can be seen at the end of Stage 2b, where it increases to about 0.1mg/L. The top observation point initially starts at <0.0mg/L then starts to increase after 20 days reaching a peak of 0.2mg/L which then steadily declines for the remainder of the simulation.

In Mix-4 the initial and second simulations have similar results, as shown in **Figure 17** and **Figure 18** respectively, with all three observations starting at 2.2mg/L, the base observation point is maintained at this concentration throughout both simulations. The middle observation in both

showed a decline in concentration from 2.2mg/L to 1.3mg/L in Stage 2a. This continued to decline in Stage 2b to 0.5mg/L. The top observation is very similar to the profile of the top observation of Mix-2, however, at a magnitude higher. In the final simulation of Mix-4, see **Figure 19**, the concentration for all three observation points started at 0.6mg/L. this increased in a step wise fashion to 1.4mg/L at 30 days, where it then began to decline slightly for the remainder of the simulation to 1.3mg/L. The middle and base observations both maintained a concentration of 0.6mg/L, at 50 days the middle begins to increase slightly while the base maintained its current concentration for the remainder of the simulation.

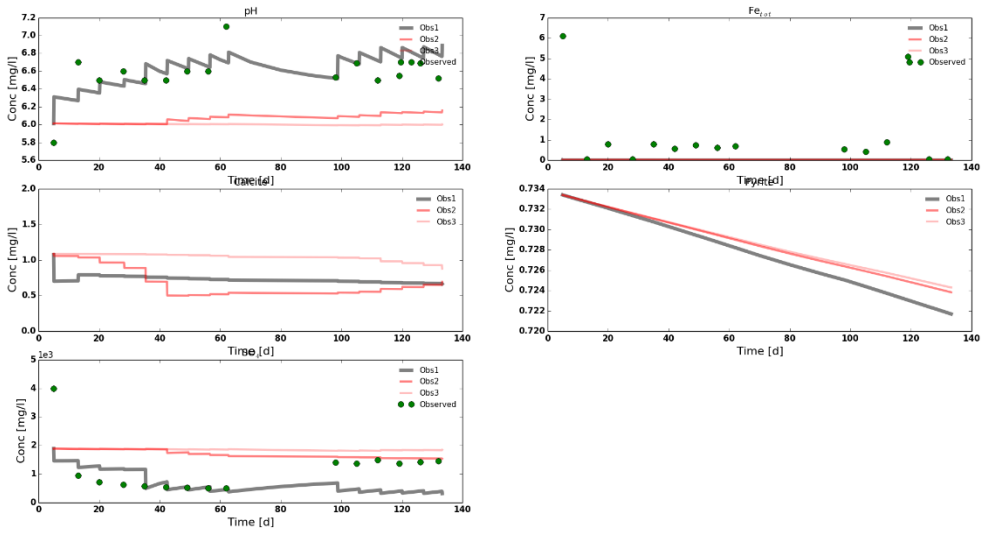

Figure 21. Simulated results from the second simulation of Mix-6 showing concertation over time for pH (top left), total Fe (top right), Calcite (middle left), pyrite (middle right) and sulphate (bottom left). Green dot are the observed results from the column experiments conducted.

In both the initial and second simulation of column Mix-6 all three observations points showed a concentration of 1.1 to begin with as seen in **Figure 20** and **Figure 21** respectively. The top observation has a sharp decline initially to 0.7mg/L, where it continues to decline at a slower rate for the remainder of the simulation. The middle observation declines to 0.5mg/L in the first 40 days then begins to rise slowly for the remainder for the simulation. The base observation has a very slow decline over the entire simulation to a concentration of 0.9mg/L with most of the change happening in the last 30 days of the simulation (see **Figure 20** and **Figure 21**). In the final run of Mix-6, **Figure 22** shows all three observation points started with a concentration of 0.5mg/L. The top observation had a rise in the first 20 days to 0.8mg/L which then slowly declined for the remainder of the simulation. The middle and base observations maintained the concentration of 0.5mg/L till the end of Stage 2a, where the middle observation began to rise in concentration to 0.8mg/L by the end of the simulation.

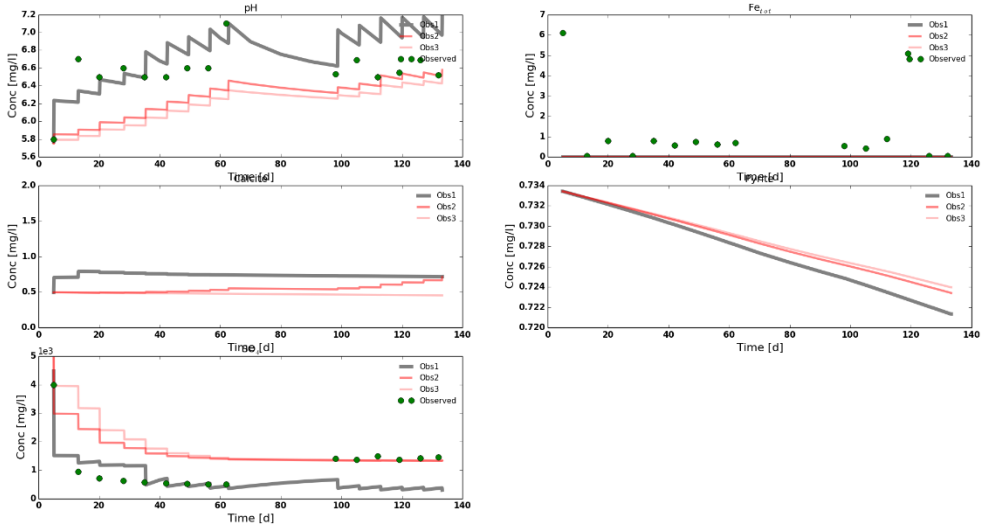

Figure 22. Simulated results from the final simulation of Mix-6 showing concertation over time for pH (top left), total Fe (top right), Calcite (middle left), pyrite (middle right) and sulphate (bottom left). Green dot are the observed results from the column experiments conducted.

6.2 WR mixes

6.2.1 pH

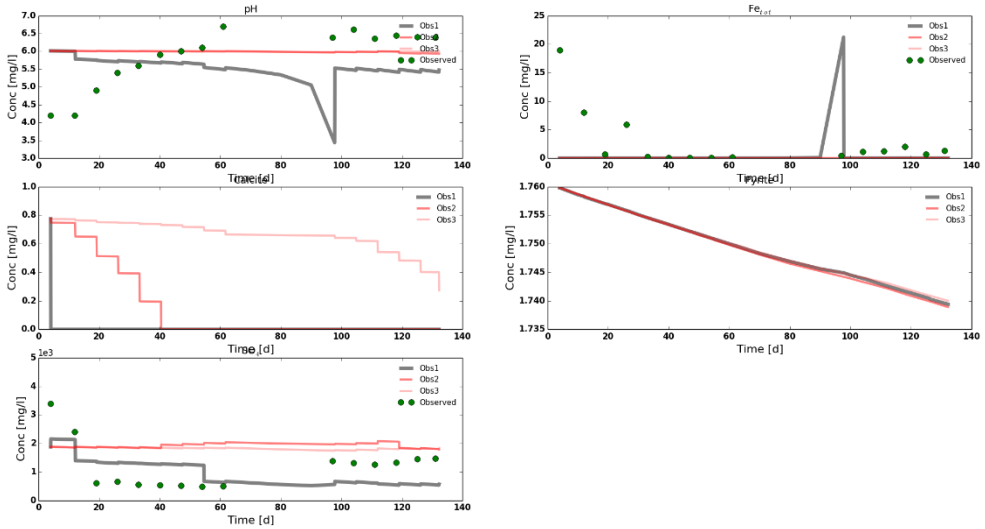

Figure 23. Simulated results from the initial simulation of WR-2 showing concertation over time for pH (top left), total Fe (top right), Calcite (middle left), pyrite (middle right) and sulphate (bottom left). Green dot are the observed results from the column experiments conducted.

The WR columns in the initial simulation all displayed the same pH at the base and the middle observation points at pH 6. The exception to this was WR(1.2)-2 which displayed a base pH that is very low compared to the observed pH 2.5, as seen in **Figure 29**. The initial simulation for WR(1.2)-2 also displayed the top rising to a pH 5.5, then falling to pH 3.5. The rise and fall observed occurs with sampling and refilling events throughout the simulation (see **Figure 29**). WR-2 columns top

observation was consistently lower than the middle and base observations, reaching pH 3.1 at its lowest during the intermission between Stage 2a and Stage 2b. As observed in **Figure 35**, WR(4)-2 the top observation displayed a rise in a step like fashion above the base pH in Stage 2a, which changed to a rise and fall spike in Stage 2b. Rising to pH 6.3 and falling below the base observation pH in each cycle (see **Figure 35**). The three WR columns WR-4, WR(1.2)-4 and WR(4)-4, all displayed similar profiles for the top pH, with a constant small rise and fall (see **Figures 26, 32 and 38** respectively). The observed pH from the column experiment is significantly different to the simulated pH across all WR columns simulated.

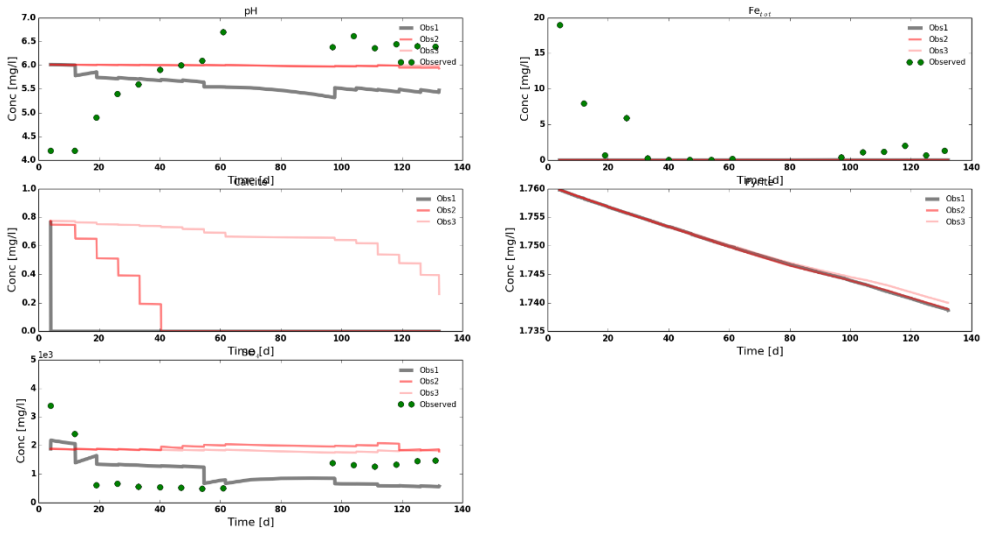

Figure 24. Simulated results from the second simulation of WR-2 showing concertation over time for pH (top left), total Fe (top right), Calcite (middle left), pyrite (middle right) and sulphate (bottom left). Green dot are the observed results from the column experiments conducted.

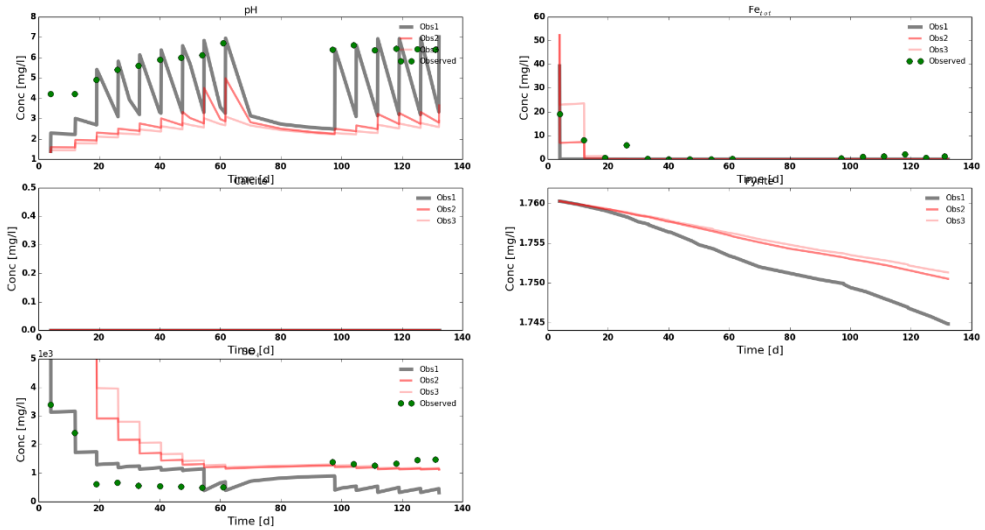

Figure 25. Simulated results from the final simulation of WR-2 showing concertation over time for pH (top left), total Fe (top right), Calcite (middle left), pyrite (middle right) and sulphate (bottom left). Green dot are the observed results from the column experiments conducted.

In the second simulation of the WR columns, the base pH simulated was very similar to the initial run for all the columns, except WR(1.2)-2. The base pH was simulated as dropping and rising from pH 5.5 to pH 3.0 compared to the top pH that was dropping and rising in the initial simulation (see **Figure 30**). The top observation displayed a pH in WR(1.2)-2 that varied slightly, ranging from pH 5.5 to pH 5.2 until the intermission. There is a drop to pH 3.0, however, this drop is quickly recovered in Stage 2b (see **Figure 30**). The remainder of the columns were similar in the profile to the initial simulation for the middle and top observation points, with some slight variation in Stage 2b. As in the first simulation the observed pH from the column experiment is significantly different to the simulated pH across all the WR columns.

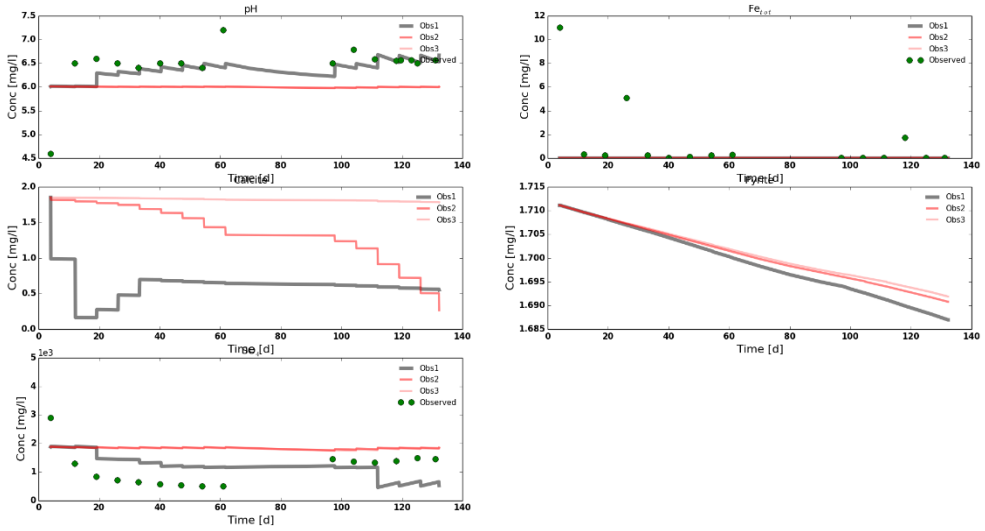

Figure 26. Simulated results from the initial simulation of WR-4 showing concertation over time for pH (top left), total Fe (top right), Calcite (middle left), pyrite (middle right) and sulphate (bottom left). Green dot are the observed results from the column experiments conducted.

In the final simulation there is a significant change in the profiles of the simulated pH in the WR columns. In WR-2 the pH starts significantly lower, at pH 2.0, then begins to rise and match the observed results in the second half of Stage 2a as seen in **Figure 25**. In Stage 2b the base pH is slow to rise, not reaching observed results. The pH simulated in WR-4, rises over time with refilling events from pH 5.5 to pH 6.6 (see **Figure28**). The end of Stage 2a and the majority of Stage 2b the simulated results at the base observation match up with the observed results from the column experiment. WR(4)-2 the simulated pH start at pH 5.3 and rises in a step wise fashion as observed in **Figure 37**. This is a similar profile to WR(4)-4, **Figure 40**, though the observed results are lower than the simulated results for the entire simulation. In WR(4)-4 the pH starts at pH 5.5, rising in a step wise fashion, reaching similar results to the observed results. A drop is observed in the simulation at the intermission between Stage 2a and Stage 2b which resulted in the pH being slightly more out in Stage 2b as seen in **Figure 40**, however the simulated results are still like the observed results. Column WR(1.2)-4 has simulated results that display a profile like WR(4)-4, although, the pH in Stage 2a is different than the observed results, and Stage 2b is more comparable to the observed results

(see **Figure 34**). The final column WR(1.2)-2, displayed a similar pH to WR-2 at pH 1. Though in this column the rise across all observation points was slower as observed in **Figure 31**. Stage 2b was like WR-2 across all observation points. There was no similarity between the simulated and observed pH in this column.

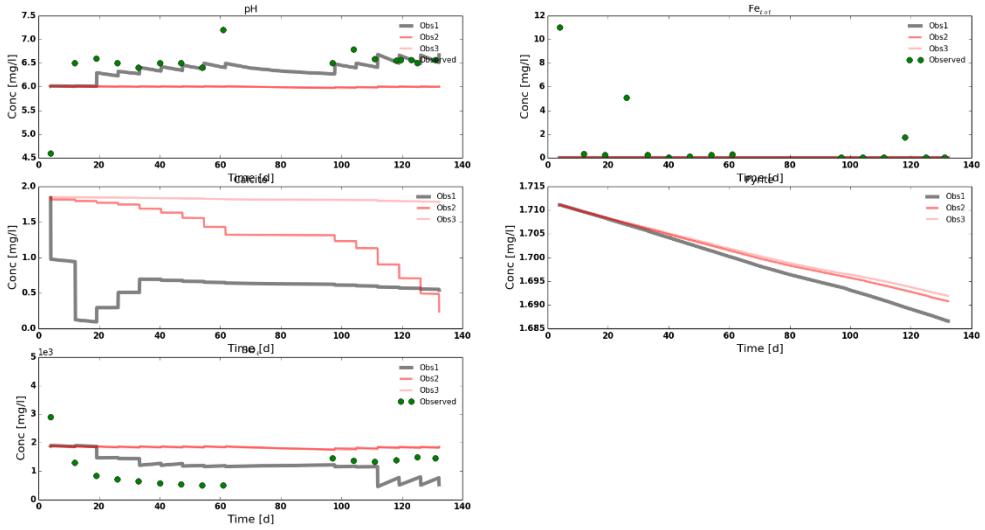

Figure 27. Simulated results from the second simulation of WR-4 showing concertation over time for pH (top left), total Fe (top right), Calcite (middle left), pyrite (middle right) and sulphate (bottom left). Green dot are the observed results from the column experiments conducted.

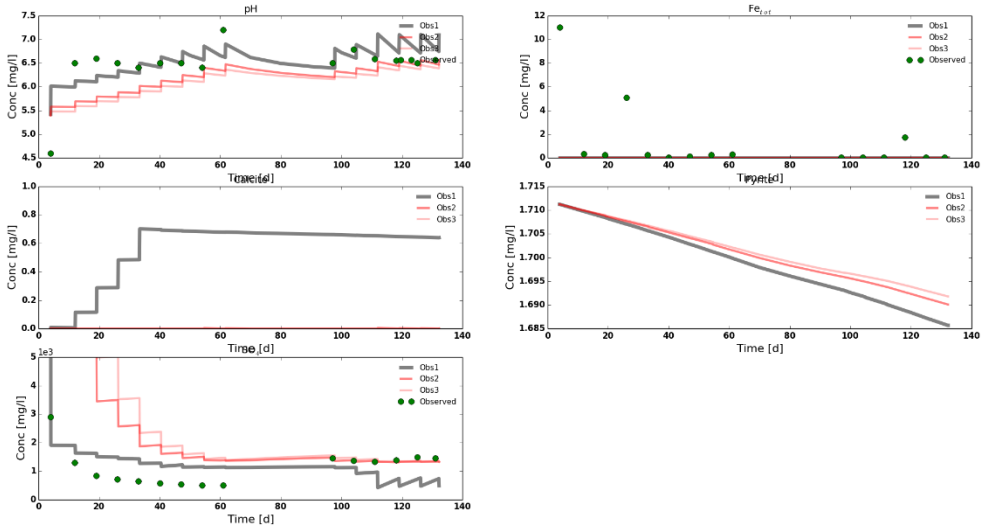

Figure 28. Simulated results from the final simulation of WR-4 showing concertation over time for pH (top left), total Fe (top right), Calcite (middle left), pyrite (middle right) and sulphate (bottom left). Green dot are the observed results from the column experiments conducted.

6.2.2 SO_4^{2-}

The initial run of the WR columns showed that SO_4^{2-}at the base of WR(1.2)-2 starts with a concentration of 1100mg/L and has a slight increase by the end of stage 2b. The simulated results

are close in concentration to the observed results in Stage 2b (see **Figure 29**). The top observation shows sulphate that is less than 1000mg/L for the whole simulation. The remaining WR columns – WR(1.2)-4, WR(4)-4, WR(4)-2, WR-4 and WR-2 – all have SO_4^{2-}concentrations at the base and middle that are at 2000mg/L, this is slightly higher than the observed concentrations in Stage 2b and a magnitude higher in Stage 2a. The top observation shows concentrations that are less than 2000mg/L, apart from WR-2 and WR(4)-2, which both have a small spike at the beginning of the simulation.

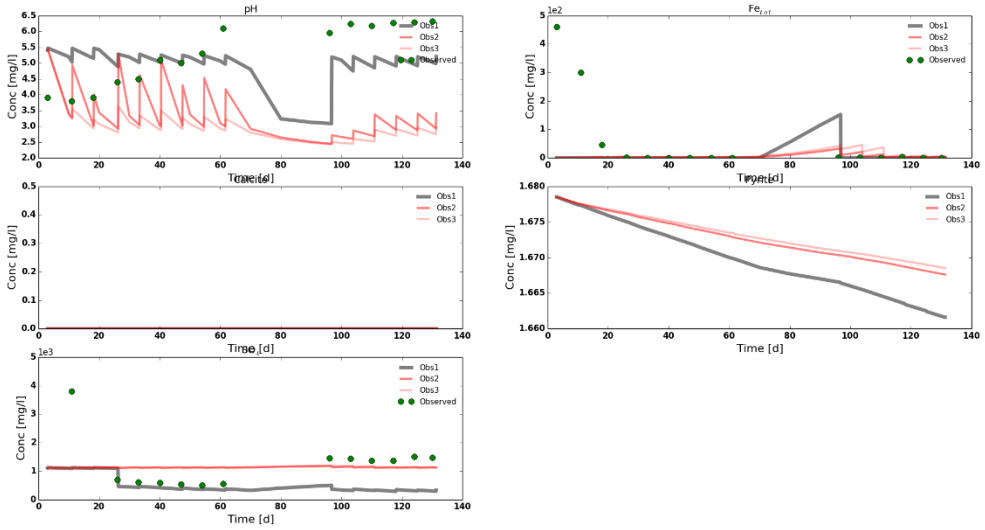

Figure 29. Simulated results from the initial simulation of WR(1.2)-2 showing concertation over time for pH (top left), total Fe (top right), Calcite (middle left), pyrite (middle right) and sulphate (bottom left). Green dot are the observed results from the column experiments conducted.

The SO_4^{2-} concentrations in WR columns in the second simulation are very similar in the general profile of the initial run. The notable differences are that there is a small fluctuation in the simulated results of all columns in Stage 2b. Though the simulated results are still higher than the observed results. Another notable change is that in WR-2 and WR(4)-2, **Figure 24** and **Figure 36** respectively, the small spike in the SO_4^{2-} concentration that occurred in the initial run is now earlier.

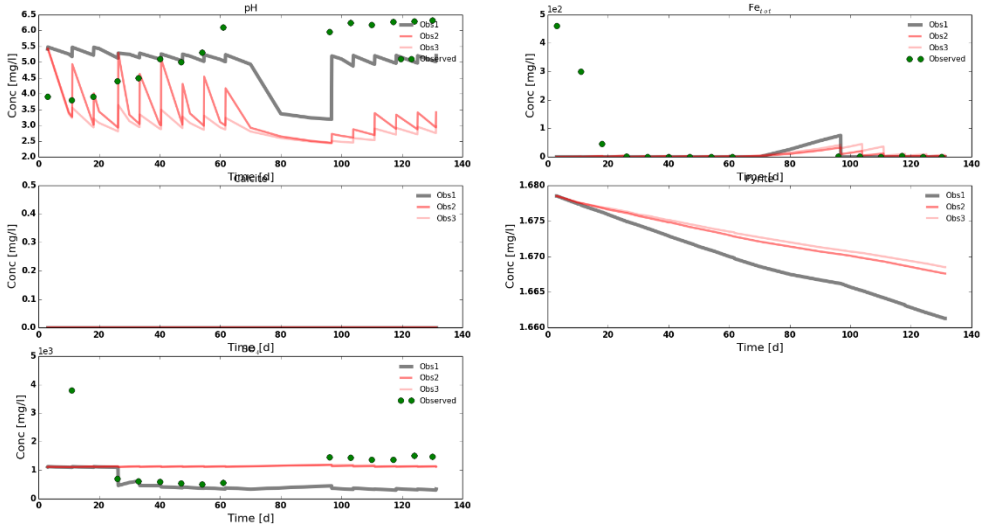

Figure 30. Simulated results from the second simulation of WR(1.2)-2 showing concertation over time for pH (top left), total Fe (top right), Calcite (middle left), pyrite (middle right) and sulphate (bottom left). Green dot are the observed results from the column experiments conducted.

In the final run of the WR columns the SO_4^{2-} concentrations simulated at all three observation sites, top middle and base, was above 5000mg/L. This dropped to 1000mg/L in all column's half way though Stage 2a, at all three observation points. The SO_4^{2-} concentration in Stage 2b is very close to the observed results for all WR columns. However, Stage 2a is now several magnitudes higher than the observed results.

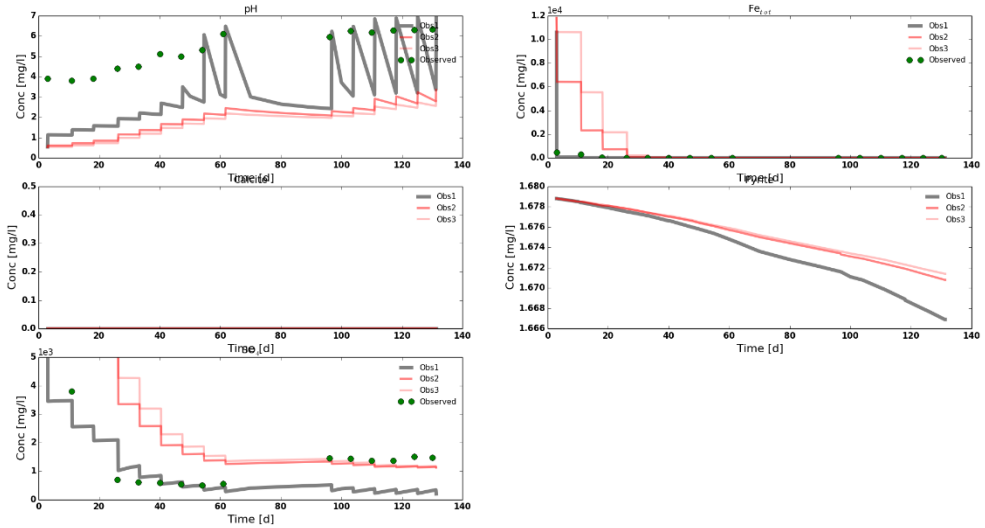

Figure 31. Simulated results from the final simulation of WR(1.2)-2 showing concertation over time for pH (top left), total Fe (top right), Calcite (middle left), pyrite (middle right) and sulphate (bottom left). Green dot are the observed results from the column experiments conducted.

6.2.3 Total Fe

For the initial simulation both WR-2 and WR(1.2)-2, **Figure 23** and **Figure 29** respectively, both have simulated result that were excessive compared to observed results. The remainder of the WR columns had simulated results at trace concentrations at <0.0mg/L. Column WR-2 had a spike in Fe concentration though the intermission between Stage 2a and Stage 2b, where the concentration got to 180mg/L as observed in **Figure 23**. In WR(1.2)-2 the Fe concentration showed rising and falling at the beginning of Stage 2a, with the base getting to a concentration of 100mg/L and increasing to 250mg/L after the intermission.

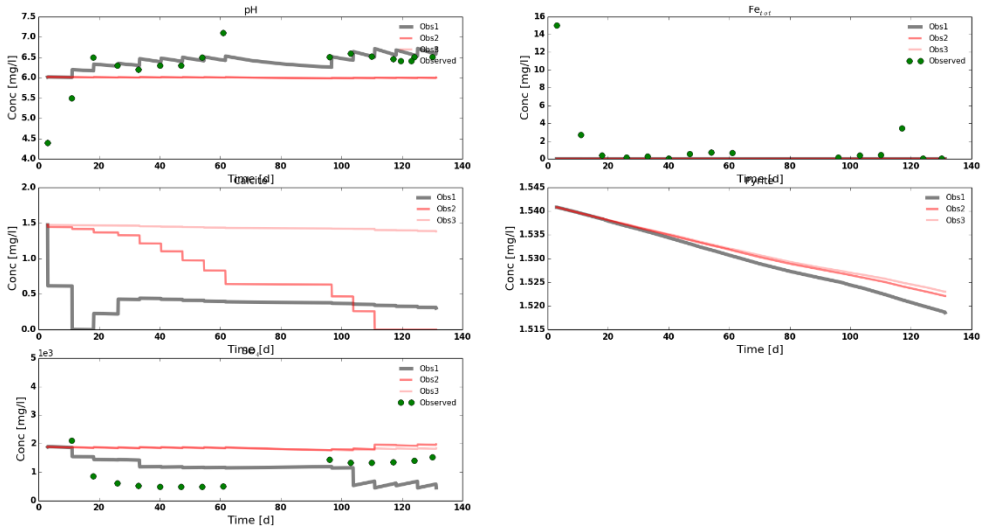

Figure 32. Simulated results from the initial simulation of WR(1.2)-4 showing concertation over time for pH (top left), total Fe (top right), Calcite (middle left), pyrite (middle right) and sulphate (bottom left). Green dot are the observed results from the column experiments conducted.

The second simulation also produced Fe concentrations at <0.0mg/L in all columns with the exception of WR(1.2)-2 which displayed a small rise to 100mg/L in the intermission in all three

observation points. This quickly returned to trace concentrations once sampling recommenced in Stage 2b (see **Figure 30**).

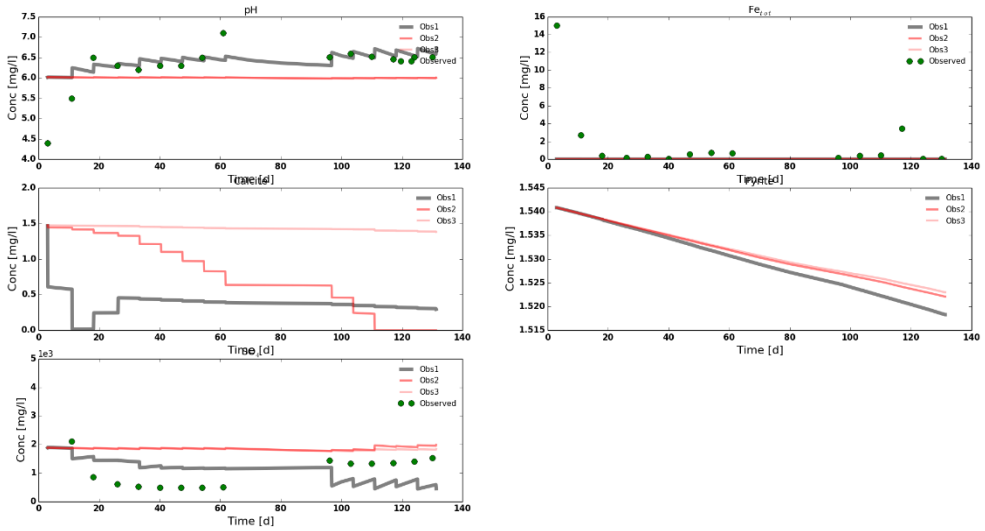

Figure 33. Simulated results from the second simulation of WR(1.2)-4 showing concertation over time for pH (top left), total Fe (top right), Calcite (middle left), pyrite (middle right) and sulphate (bottom left). Green dot are the observed results from the column experiments conducted.

In the final simulation, all of the WR columns had a concentration of <0.0mg/L which is close to observed concentrations, the exception to this was WR-2 and WR(1.2)-2. With WR-2 having a spike at the beginning of around 50mg/L which quickly reduced to trace concentrations, very similar to the observed as seen in **Figure 25**. Column WR(1.2)-2 was the same but with an initial concentration of 12000mg/L, see **Figure 31**, this took slightly longer to reduce to trace concentrations.

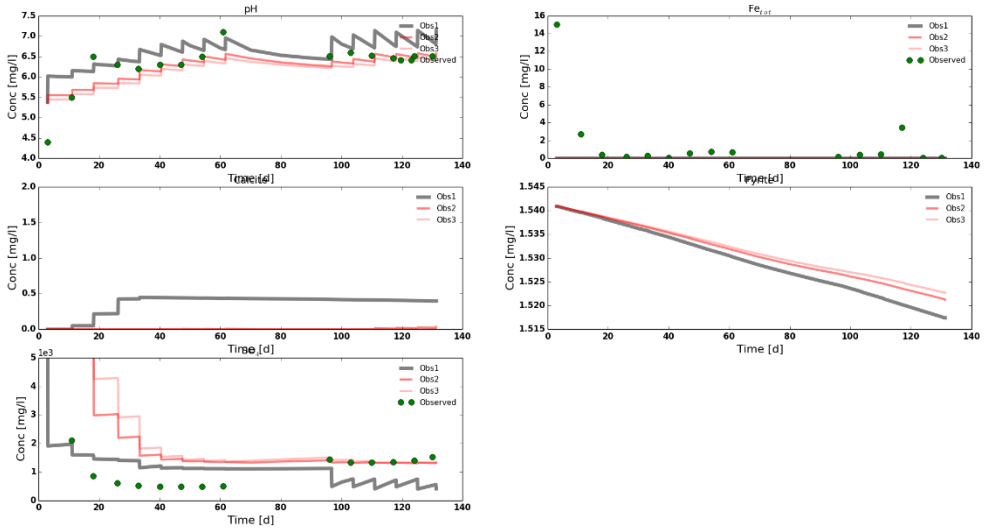

Figure 34. Simulated results from the final simulation of WR(1.2)-4 showing concertation over time for pH (top left), total Fe (top right), Calcite (middle left), pyrite (middle right) and sulphate (bottom left). Green dot are the observed results from the column experiments conducted.

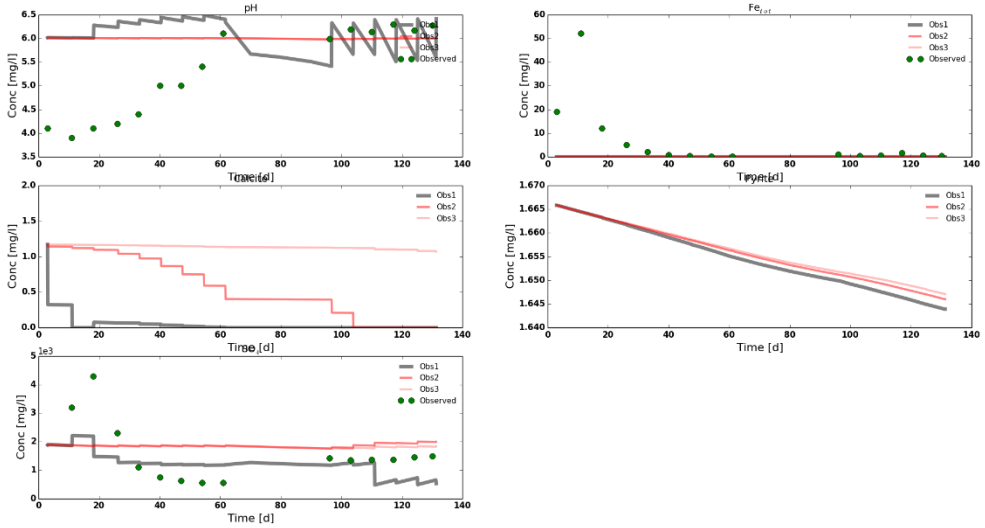

Figure 35. Simulated results from the initial simulation of WR(4)-2 showing concertation over time for pH (top left), total Fe (top right), Calcite (middle left), pyrite (middle right) and sulphate (bottom left). Green dot are the observed results from the column experiments conducted.

6.2.4 FeS_2

In the initial simulation of the WR columns many had a dissolution of FeS_2 at the base observation of between 1% and 2% of the wt.%. There was two columns, WR-4 and WR(1.2)-2 that both had < 1% of the wt.% that was dissolved throughout the simulation. It is noted that all the columns did have a spread in the concentrations at the three observation points. Column WR(1.2)-4 base and middle observations were closer together that the rest of the columns.

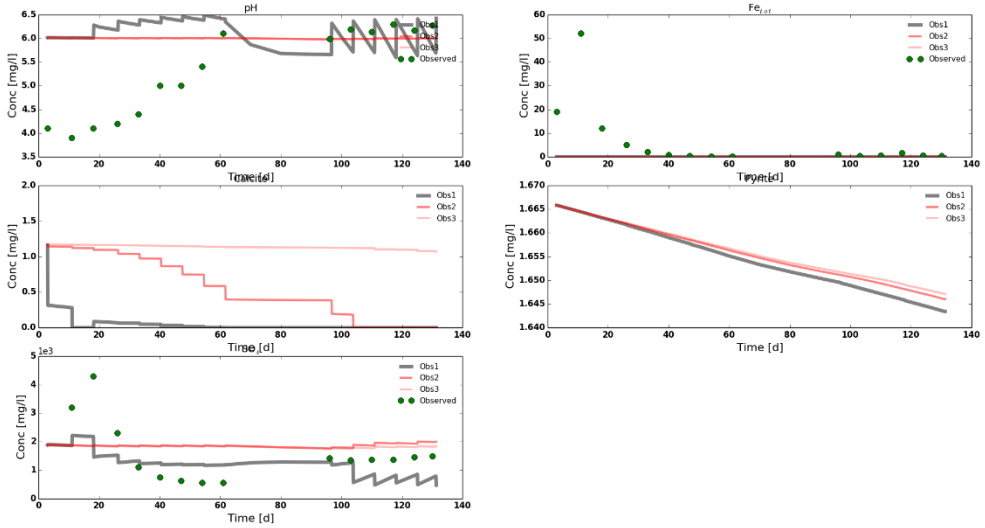

Figure 36. Simulated results from the second simulation of WR(4)-2 showing concertation over time for pH (top left), total Fe (top right), Calcite (middle left), pyrite (middle right) and sulphate (bottom left). Green dot are the observed results from the column experiments conducted.

The FeS_2 dissolution at the base of the column in the second simulation is analogous to the initial simulation. However, WR-4 is the only column that had a dissolution of < 1% of the wt.%, see **Figure 27**. The spread of FeS_2 dissolution throughout the column has also changed compared to the initial simulation. With columns WR-4, WR(4)-4, WR(1.2)-2 and WR(1.2)-4 all having the base and middle observations showing similar concentrations of FeS_2 . While WR-2 and WR(4)-2 both show all three observation points with similar FeS_2 concentrations.

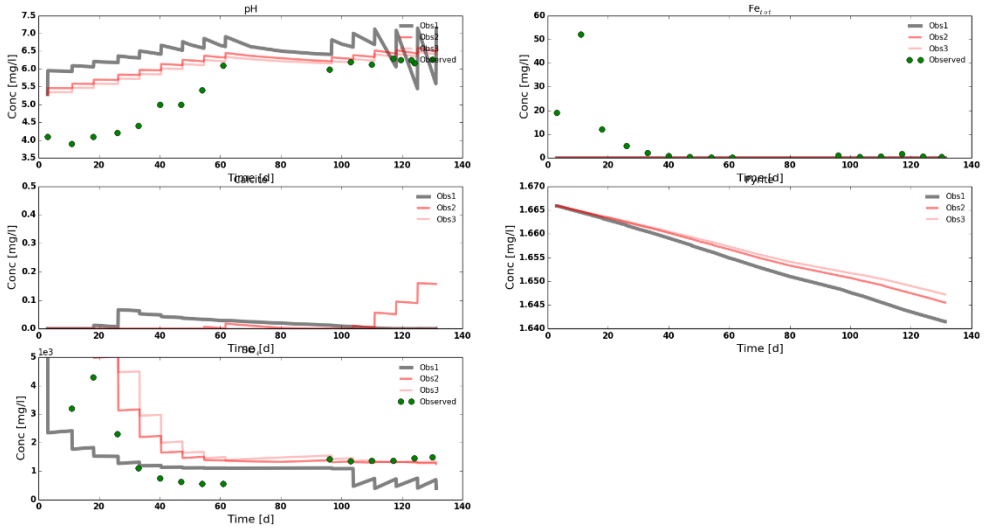

Figure 37. Simulated results from the final simulation of WR(4)-2 showing concertation over time for pH (top left), total Fe (top right), Calcite (middle left), pyrite (middle right) and sulphate (bottom left). Green dot are the observed results from the column experiments conducted.

The final simulation of the WR columns showed that the majority of the columns had between 1% and 2% wt.% dissolution of FeS_2 . Columns WR-2 and WR(1.2)-2, **Figure 34** and **Figure 31** respectively, both had less than 1% wt.% of FeS_2 dissolution. Three of the columns displayed similar profiles at all three observations points to the second simulation, WR(1.2)-4, WR(4)-4 and WR-4, **Figures 34, 40 and 28**, with base and middle FeS_2 concentrations been similar. Column WR-2 showed a greater spread between the three observation points than the second simulation. However, middle and base concentrations were still similar, as was WR(1.2)-2.

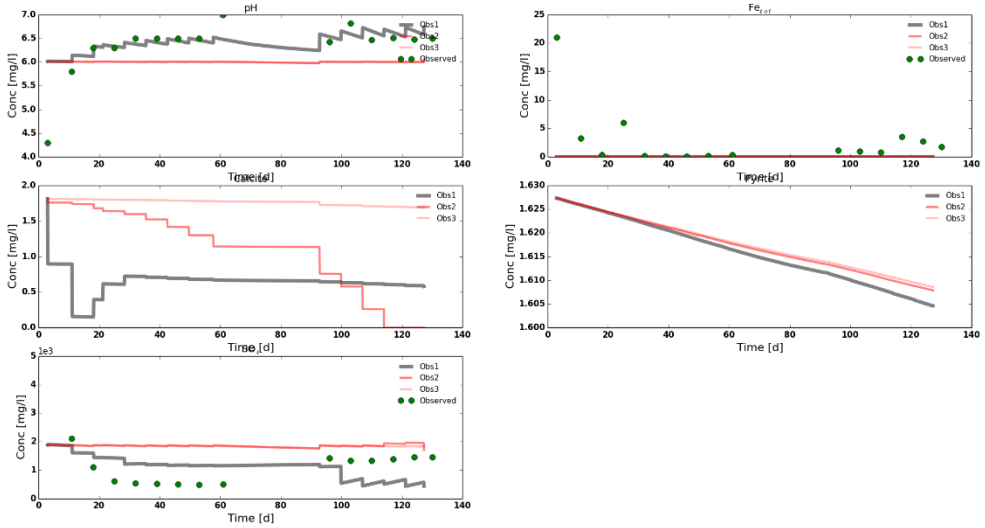

Figure 38. Simulated results from the initial simulation of WR(4)-4 showing concertation over time for pH (top left), total Fe (top right), Calcite (middle left), pyrite (middle right) and sulphate (bottom left). Green dot are the observed results from the column experiments conducted.

6.2.5 $CaCO_3$

As column WR(1.2)-2 had 0%wt. of $CaCO_3$ present there was no concentrations simulated in all three simulations. The initial and second simulation for WR-2 are similar, with the top observation immediately dropping from 0.8mg/L to <0.0mg/L. The middle observation point also reduces to <0.0mg/L at 40 days. The base had a slow decline until 110 days where an increase in the dissolution results in 0.3mg/L (see **Figure 23** and **Figure 24**). The final simulation shows an initial concentration of <0.0mg/L for all three observations, which is carried throughout the entire simulation. For column WR(4)-2 the initial and second simulation showed all observation points starting at 1.2mg/L, with the base having a slow decline to 1.0mg/L. The middle observation has a drop in a step wise fashion from 1.2mg/L to 0.5mg/L in Stage 2a. In Stage 2b this continues to drop to <0.0mg/L. The top observation declines rapidly to 0.1mg/L in 20 days, then slowly to <0.0mg/L over the remainder of the simulation as seen in **Figure 35** and **Figure 36**. The final simulation of WR(4)-2 started with a concentration of <0.0mg/L for all three observation points, the top observation was observed having a spike to 0.1mg/L, and slowly declining to <0.0mg/L. The middle observation had a rise in Stage 2b

at 110 days, which continued to rise until the end of the simulation, reaching a concentration of 0.18mg/L.

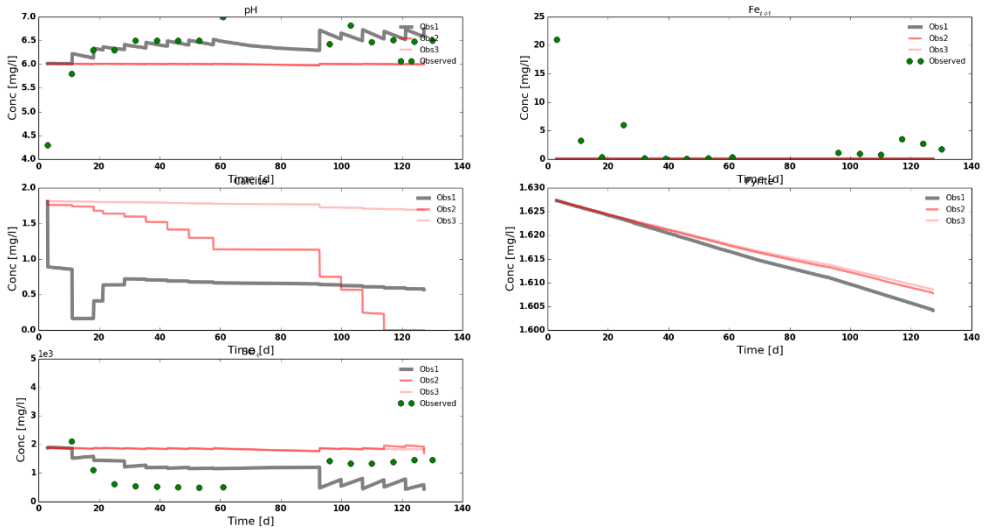

Figure 39. Simulated results from the second simulation of WR(4)-4 showing concertation over time for pH (top left), total Fe (top right), Calcite (middle left), pyrite (middle right) and sulphate (bottom left). Green dot are the observed results from the column experiments conducted.

The simulated column of WR-4 showed that in the initial simulation, **Figure 26**, and second simulation, **Figure 27**, started with a concentration of $CaCO_3$ at 1.9mg/L. The base observation was maintained at a constant concentration throughout the simulation, while the middle observation had a step-down drop to <0.0mg/L at 110 days. The top observation has an initial drop to 0.2mg/L then rise to 0.7mg/L at 35 days, then slowly declined for the remainder of the simulation reaching a concentration of 0.5mg/L. In the final simulation of WR-4 all three observations start at <0.0mg/L, as observed in **Figure 28**, with the top observation increasing in Stage 2a, reaching a concentration of 0.8mg/L . There is no observed increase in concentration at the base or middle observation points. The initial and second simulation for column WR(1.2)-4, the concentration starts at 1.5mg/L for all three observation points, see **Figure 32** and **Figure 33** respectively. The middle observation point declines throughout the simulation reaching <0.0mg/L at 110 days. The top observation initial declines then increase to 0.5mg/L, at which point it begins to slowly decline for the remainder of the simulation. **Figure 34** shows the final simulation for WR(1.2)-4, which is similar to the final simulation of WR-4 with the top observation reaching a concentration of 0.5mg/L at 30 days, then declining for the remainder of the simulation. In WR(4)-4 the initial and second simulations, (**Figure 38** and **Figure 39**) are similar to WR(1.2)-4 though the initial concentration starts higher at 1.8mg/L. In the final simulation the top observation increases to 0.8mg/L by 30 days then slowly decreases for the

remainder of the simulation. The middle observation also has a slight increase towards the end of Stage 2b.

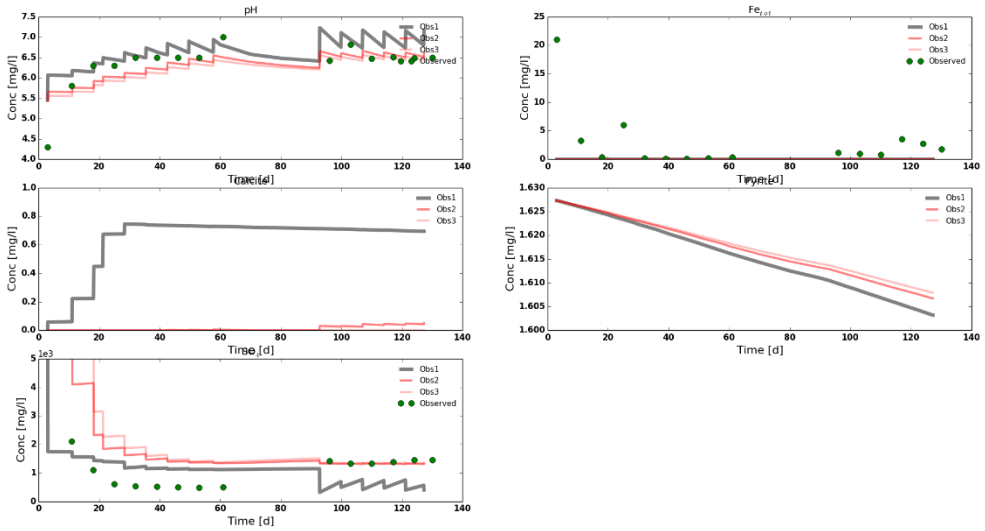

Figure 40. Simulated results from the final simulation of WR(4)-4 showing concertation over time for pH (top left), total Fe (top right), Calcite (middle left), pyrite (middle right) and sulphate (bottom left). Green dot are the observed results from the column experiments conducted.

6.3 Tailings mixes

6.3.1 pH

The initial simulation of the column T-2 started at pH 6.0 while the observed pH was at 4.0 as shown in **Figure 41**. Observations at the top of the simulated column show the pH rising over time with sampling and refiling periods, while the observations at the base and middle of the column show no change, with the base staying at pH 6.0 and the middle having a small rise to pH 6.25. The same can be seen in the simulation of T-4, see **Figure 44**, however the overall rise of the pH at the top observation marginally higher. The second simulation of both T-2 and T-4 have very identical profiles, as observed in **Figure 42** and **Figure 44** respectively. The top observation points of T-4 had a slightly higher simulated pH than the T-2 column. In both runs the middle and base observations points showed simulated a pH starting at pH 6.0 and rising slowly to around a pH 6.6 in Stage 2a. This rise is very similar to observed results from the column experiments as viewed in **Figure 42** and **Figure 45**. The same is observed in Stage 2b in both T-2 and T-4, with simulated results of pH similar to the observed results of pH. In the final simulation of T-2 and T-4 there is minimal change in the simulated results from the second simulation, with the base and middle observations been closer in simulated pH to the observed pH as seen in **Figure 43** and **Figure 46** respectively.

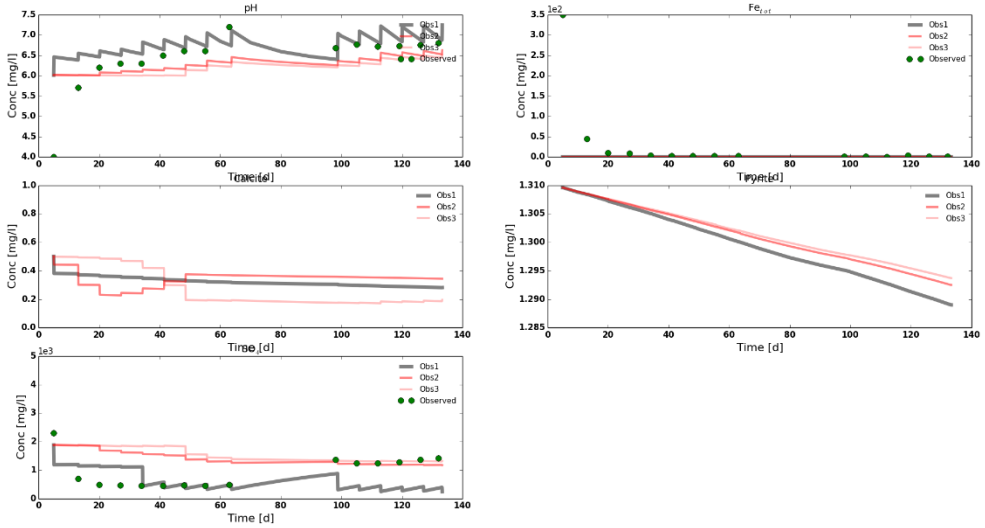

Figure 41. Simulated results from the initial simulation of T-2 showing concertation over time for pH (top left), total Fe (top right), Calcite (middle left), pyrite (middle right) and sulphate (bottom left). Green dot are the observed results from the column experiments conducted.

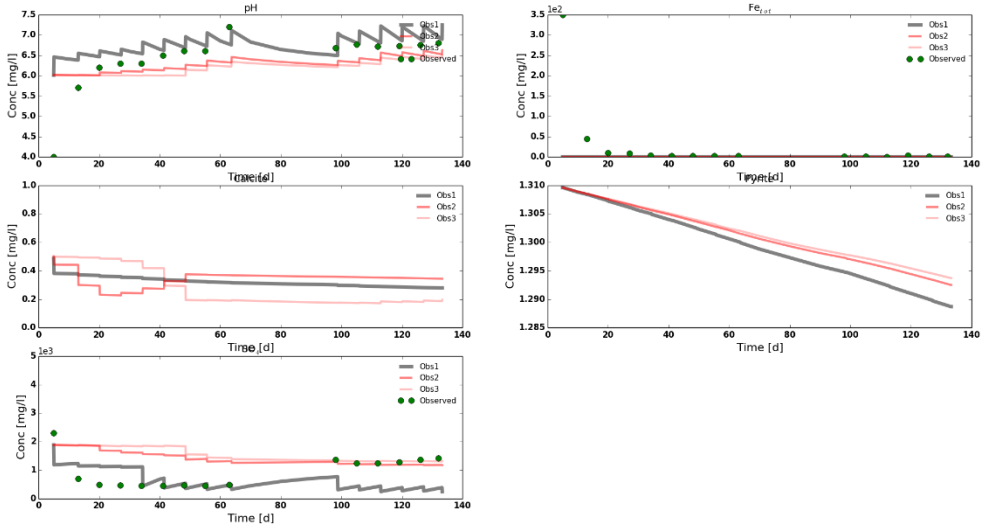

Figure 42. Simulated results from the second simulation of T-2 showing concertation over time for pH (top left), total Fe (top right), Calcite (middle left), pyrite (middle right) and sulphate (bottom left). Green dot are the observed results from the column experiments conducted.

6.3.2 SO_4^{2-}

The SO_4^{2-} in both T-2 and T-4 starts at a concentration of 2000mg/L at all three observation points, top middle and base, in the initial run. However, in T-4 the top observation point drops to around 500mg/L, this coincides with the sampling and refilling periods as seen in **Figure 44**. In both T-2 and T-4 columns the simulated concentrations are a magnitude higher than the observed results in Stage 2a. Stage 2b shows simulated results from both T-2 and T-4 that are closer to the observed results from the columns experiments, at a concentration of around 1900mg/L (see **Figure 41** and **Figure**

44). In the second simulation the concentrations for both T-2 and T-4 also starts at 2000mg/L. However, this decline to around 1500mg/L by the end of Stage 2a. Although the simulated concentrations are still a magnitude higher than the observed concentrations for both T-2 and T-4 columns as viewed in **Figures 42** and **Figure 45**. This decline of the SO_4^{2-} brings the simulated concentration and the observed results closer than the initial run in Stage 2b. In the final simulation for both T-2 and T-4 the SO_4^{2-} concentrations seem to start higher than the previous simulations, however they still drop to around 1500mg/L at 30 days. In **Figures 43** and **Figure 46**, the overall profile of the simulated results is similar to the second run with Stage 2b showing simulated results like the observed results at the base of the column.

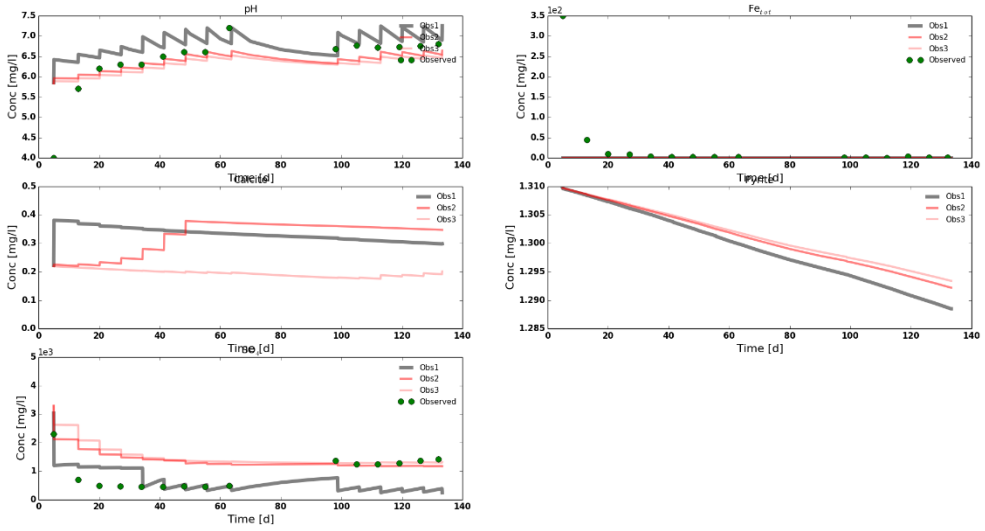

Figure 43. Simulated results from the final simulation of T-2 showing concertation over time for pH (top left), total Fe (top right), Calcite (middle left), pyrite (middle right) and sulphate (bottom left). Green dot are the observed results from the column experiments conducted.

6.3.3 Total Fe

In the initial run of T-2 and T-4 the total Fe concentrations simulated are extremely low compared to the observed results in the first 20 days, being several magnitudes higher, after this the simulated and observed results are similar. The second and final simulations have the exact same profile as the initial run as can be observed in **Figures 41, 42 and 43** for T-2 and **Figures 44, 45 and 46** for T-4.

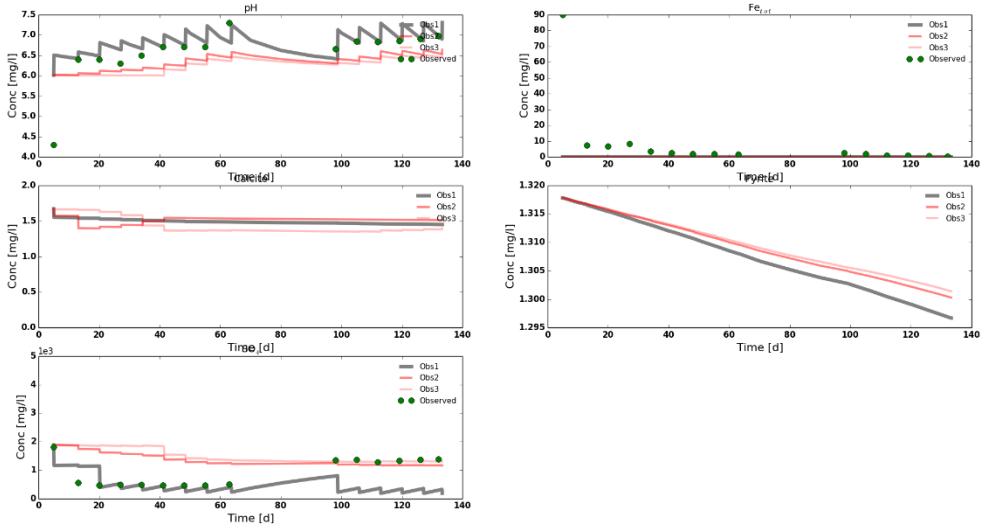

Figure 44. Simulated results from the initial simulation of T-4 showing concertation over time for pH (top left), total Fe (top right), Calcite (middle left), pyrite (middle right) and sulphate (bottom left). Green dot are the observed results from the column experiments conducted.

6.3.4 FeS_2

For all three simulation in both T-2 and T-4 columns there was no change in the profile or concentration of FeS_2 from one simulation to the next. All of simulations showed dissolution of FeS_2 slightly greater than 2% of the wt.% of the column.

6.3.5 $CaCO_3$

The initial and second simulation results are the same from column T-2, with all three observation points starting at a concentration of 0.5mg/L. The top observation shows a decline in concentration throughout the simulation. The middle observation shows more rapid decline which then starts to increase at 30 days until 50 days at which point it starts to decrease slowly. A rapid reduction in concentration at the base observation is observed from 30 days to 50 day. This reduction then continues to decline at a slower rate for the remainder of the simulation (see **Figure 41** and **Figure 42**). The final simulation of T-2 column started out with all three observation points starting at 0.21mg/L, with the top observation jumping to 0.39mg/L then starting to decline for the remainder of the simulation to 0.3mg/L. The middle observation point rises in a step wise fashion over the first 50 days to 0.39, which then declines for the remainder of the simulation to 0.35mg/L. The base observation has a slight decline throughout the entire simulation, as seen **Figure 42**.

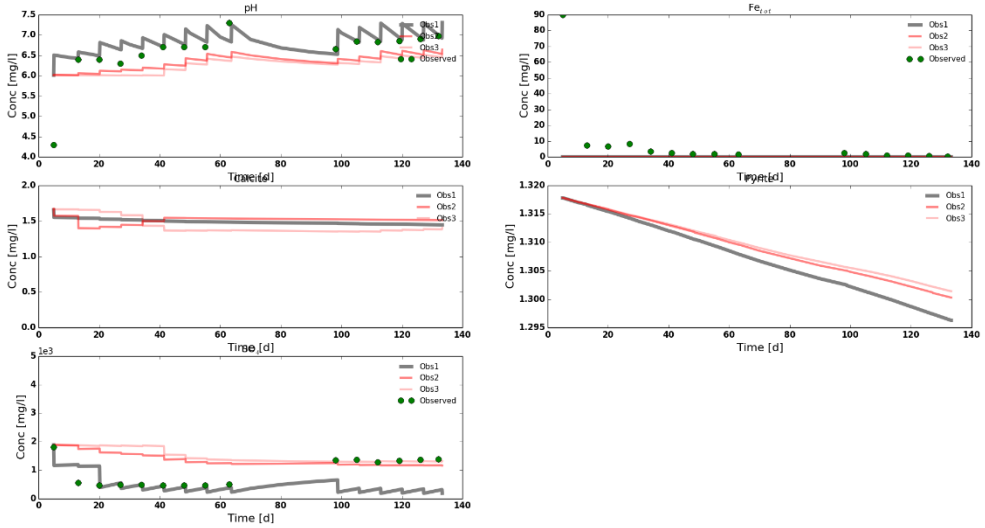

Figure 45. Simulated results from the second simulation of T-4 showing concertation over time for pH (top left), total Fe (top right), Calcite (middle left), pyrite (middle right) and sulphate (bottom left). Green dot are the observed results from the column experiments conducted.

The initial and second simulation are very alike and display a similar profile to the initial and second simulations of T-2 columns, however, the range is smaller as seen in **Figure 44** and **Figure 45**. The starting concentration is 1.6mg/L and the final concentration at 1.5mg/L. The final simulation for the T-4 column shows that the concentration at all three observation points started at 1.4mg/L and had some subtle changes in the middle and top observations. With the final concentration at the end of stage 2b at 1.5mg/L for all three observation points.

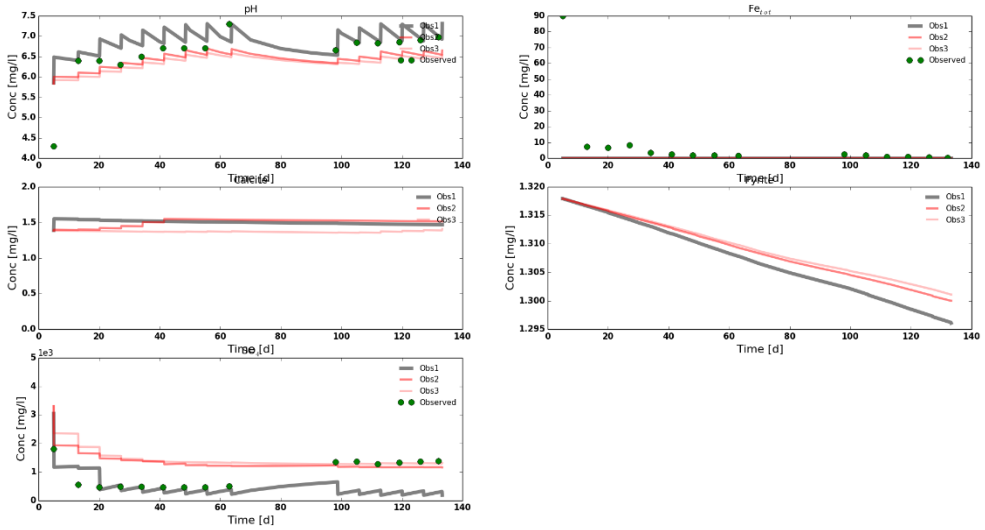

Figure 46. Simulated results from the final simulation of T-4 showing concertation over time for pH (top left), total Fe (top right), Calcite (middle left), pyrite (middle right) and sulphate (bottom left). Green dot are the observed results from the column experiments conducted.

Chapter 7 Discussion

7.1 Comparison of Model Simulations and Key Parameters

From each of the simulations that was run for each of the columns the final simulation is the most accurate at attempting to model the processes occurring in the columns from the experiment. The addition of the two minerals goethite and haematite assisted in obtaining simulated parameters close to the observed. This is noted in the pH across most of the columns. Although the exact profile of the pH evolution throughout Stage 2a cannot be replicated there is some resemblance in a number of simulations, in particular Mix-0, Mix-4, WR4, WR(1.2)-4, WR(4)-4, T-2 and T-4 (see **Figures 13, 19, 28, 40, 43 and 46** respectively).

The SO_4^{2-} concentration was also most accurately represented in the final simulation. Again, the addition of the minerals goethite and haematite have added increased accuracy. As with the pH the initial and second simulation of most of the columns was similar with little change. However, in the final simulated concentration of SO_4^{2-} does not get reduced in Stage 2a to the observed concentrations. This gives rise to other reactions that may be occurring to reduce the SO_4^{2-} so rapidly at the beginning.

The total Fe in the column experiments displayed excessively high concentrations at the beginning which rapidly reduced to trace concentrations by the end of Stage 2a, however this was not able to be simulated in the modelled columns. Each of the simulations failed to give total Fe concentrations, indicating that there is a critical reaction that controls the amount of Fe release that is not included or considered. The inclusion of the two minerals goethite and haematite, both release Fe though dissolution as shown in the reactions below in **Equation 22** and **Equation 24**3respectively. However, even with the addition of these minerals concentrations of Fe are still not reached during the simulated columns.

Equation 20. $$FeOOH + 3H^+ = Fe^{3+} + 2H_2O$$

Equation 21. $$Fe_2O_3 + 6H^+ = 2Fe^{3+} + 3H_2O$$

$CaCO_3$ dissolution displayed an opposite trend to the other parameters observed. The final simulation displayed dissolution of $CaCO_3$ at the top observation point, though, the middle and base observation points showed increases in concentration (see **Figures 16, 19, 22, 25, 28, 34, 37, 40, 43 and 46**). A possible reason for this rise in $CaCO_3$ in the middle and base may be due to the presence of siderite that was included in the simulation as detailed in **Chapter 5.3**. However, Jasna et al. (2004) discus that during $CaCO_3$ dissolution, siderite may precipitate and may also assist in maintaining or increasing the pH if high ferrous iron is present. However, as outlined above the total Fe concentration is limited to trace amounts throughout the simulation for all the columns. Reactions may be occurring simultaneously at a rate high enough to produce trace amounts of Fe and maintain enough siderite for pH neutralisation, though, as the dissolution of the two minerals goethite and haematite releases Fe^{3+}, this may not be the case. It is noted that in the initial and second simulation of all the columns, the dissolution of $CaCO_3$ in the middle and base is significant, and the pH of all the columns with $CaCO_3$ present is maintained at pH 6.0 or greater.

FeS_2 dissolution is shown to be occurring throughout the column as expected, however, this dissolution rate is very slow. Two factors may contribute to this 1) other forms of FeS_2 or sulphide

bearing minerals, may exist as outlined in **Chapter 3**. These other forms of FeS_2 or sulphide bearing minerals may be more readily dissolved, this may also result in increased sulphate concentrations that are closer to the observed results, and 2) water standing times between sampling events may result in reduced dissolution of minerals present in the column.

7.2 Assumptions

There are several major assumptions that are made throughout the modelling process. The biggest assumption is the hydraulic conductivity, along with the time taken for each sample to be collected, as neither of these parameters were provided or recorded during the column experiment. Differences in the hydraulic conductivity and the time take for each sample can greatly affect the results of the model. Increased hydraulic conductivity may result in increased dissolution due to increased movement and flow around the sediment. Likewise, extended sampling time and/or reduced hydraulic conductivity may result in increased armouring of the $CaCO_3$ surface, leading to reduced dissolution and neutralisation of the leachate. The minerals and quantities present may also greatly influence the overall outcome of the model. Although key minerals where obtained from static geochemical test as outlined in **Chapter 4.1.3**, further assessment into the major minerals present in the area may result in identifying further key minerals playing part in the leachate.

7.3 Model Sensitivity

From the three simulations that were run for all the columns it has been identified that the model needs further development of the geochemical reaction model. However, it has been observed that the model is not sensitive to dispersivity and advection, with the least amount of variation arising from the initial simulation and the second simulation. It is apparent that the addition of two minerals goethite and haematite introduced the biggest change in the simulations. Therefore, as stated above in the Assumptions, further information on the minerals and quantities present would decrease sensitivity and increase the model's ability to more accurately simulate the columns, in turn identifying the key reactions that are driving the leachate at the Brukunga Mine site, particularly in relation to the SO_4^{2-} and Fe concentrations that are unable to be obtained.

Chapter 8 Conclusion

The aim of this project was to develop a model to simulate the column tests conducted on material from the Brukunga Mine site, and identify key reactions and processes occurring that are driving the leachate to help develop a 'walk away' solution. Although a model was developed for each of the columns, this was missing some key data and had some major assumptions throughout the process, however, the major outcomes from this project are outlined below;

- Of all the columns simulated Mix-4 was the most similar to the observed results – giving leachate that is neutral pH, low in SO_4^{2-}, low in total Fe, with adequate calcite remaining for future neutralisation
- Addition of minerals goethite and haematite improved the overall accuracy of the model and $CaCO_3$ may not be the only mineral neutralising the leachate, additional minerals, siderite and potentially gibbsite may be aiding in neutralisation, additional forms of sulphide bearing minerals should be considered – FeS, $FeAsS$, $CuFeS_2$, $((ZnFe)S)$ and PbS
- Further minerals need to be included to improve accuracy of the Geochemical transport model

Further studies are required to identify the key features and driving processes of the leachate at the Brukunga Mine site. An additional column test conducted in the mind set of modelling will help in resolving some of the major assumptions made. Research into the major and minor minerals present will reduce the sensitivity of the geochemical transport model.

References

AHERN, C. R. 2004. *Acid sulphate soils : laboratory methods guidelines / [Ahern, CR ; McElnea, AE ; Sullivan, LA],* Indooroopilly, Qld, Dept. of Natural Resources, Mines and Energy.

AKCIL, A. & KOLDAS, S. 2006. Acid Mine Drainage (AMD): causes, treatment and case studies. *Journal of Cleaner Production,* 14**,** 1139-1145.

APPELO, C. A. J. & POSTMA, D. 2005. Geochemistry, groundwater and pollution.

APPELO, C. A. J., VERWEIJ, E. & SCHÄFER, H. 1998. A hydrogeochemical transport model for an oxidation experiment with pyrite/calcite/exchangers/organic matter containing sand. *Applied Geochemistry,* 13**,** 257-268.

BLOWES, D. W., PTACEK, C. J., JAMBOR, J. L. & WEISENER, C. G. 2003. 9.05 - The Geochemistry of Acid Mine Drainage A2 - Holland, Heinrich D. *In:* TUREKIAN, K. K. (ed.) *Treatise on Geochemistry.* Oxford: Pergamon.

COX, R., GRINDLEY, P., TAYLOR, J. & PAPE, S. 2006. Successfully lowering the risks and costs associated with the legacy of the abandoned brukunga pyrite mine South Australia. *7th ICARD,,* Published by ASMR, 3134

CRAVOTTA III, C. A. & TRAHAN, M. K. 1999. Limestone drains to increase pH and remove dissolved metals from acidic mine drainage. *Applied Geochemistry,* 14**,** 581-606.

DELLEUR, J. W. 2006. *The Handbook of Groundwater Engineering, Second Edition*, CRC Press.

DEVLOPMENT, D. O. S. 2013. STAGE 2 Column leach test trial work - April to June 2012 Technical Note. *In:* DEVELOPMENT, S. (ed.).

EVANGELOU, V. P. 1998. Pyrite Chemistry: The Key for Abatement of Acid Mine Drainage. *In:* GELLER, W., KLAPPER, H. & SALOMONS, W. (eds.) *Acidic Mining Lakes: Acid Mine Drainage, Limnology and Reclamation.* Berlin, Heidelberg: Springer Berlin Heidelberg.

F TAYLOR, G. & C COX, R. 1980. *The Brukunga Pyrite Mine — A Field Laboratory for Acid Rock Drainage Studies*.

FETTER, C. W. 2014. *Applied Hydrogeology: Fourth Edition*.

FREEZE, R. A. & CHERRY, J. A. 1979. *Groundwater*, Prentice-Hall.

GARCIA, C., BALLESTER, A., GONZALEZ, F. & BLAZQUEZ, M. L. 2005. Factors affecting the transformation of a pyritic tailing: scaled-up column tests. *J Hazard Mater,* 118**,** 35-43.

HOUNSLOW, A. 1995. *Water quality data : analysis and interpretation,* Boca Raton, FL, Boca Raton, FL : Lewis Publishers.

JASNA, J., W., B. D., J., P. C. & ULRICH, M. K. 2004. Multicomponent reactive transport modeling of acid neutralization reactions in mine tailings. *Water Resources Research,* 40.

JOHNSON, D. B. & HALLBERG, K. B. 2005. Acid mine drainage remediation options: a review. *Sci Total Environ,* 338**,** 3-14.

JURJOVEC, J., PTACEK, C. J. & BLOWES, D. W. 2002. Acid neutralization mechanisms and metal release in mine tailings: a laboratory column experiment. *Geochimica et Cosmochimica Acta,* 66**,** 1511-1523.

KALIN, M., FYSON, A. & WHEELER, W. N. 2006. The chemistry of conventional and alternative treatment systems for the neutralization of acid mine drainage. *Science of The Total Environment,* 366**,** 395-408.

KALYONCU ERGULER, G., ERGULER, Z. A., AKCAKOCA, H. & UCAR, A. 2014. The effect of column dimensions and particle size on the results of kinetic column test used for acid mine drainage (AMD) prediction. *Minerals Engineering,* 55**,** 18-29.

KEFENI, K. K., MSAGATI, T. A. M. & MAMBA, B. B. 2017. Acid mine drainage: Prevention, treatment options, and resource recovery: A review. *Journal of Cleaner Production,* 151**,** 475-493.

KOMNITSAS, K., BARTZAS, G. & PASPALIARIS, I. 2004. Efficiency of limestone and red mud barriers: laboratory column studies. *Minerals Engineering,* 17**,** 183-194.

MCLEARY, M. B. 2009. Striving for 'walk-away' — focusing an expert group on the 'holy grail' of mine closure. *In:* FOURIE, A. B. & TIBBETT, M. (eds.) *Fourth International Conference on Mine Closure.* Perth: Australian Centre for Geomechanics.

MILLER, A., WILDEMAN, T. & FIGUEROA, L. 2013. Zinc and nickel removal in limestone based treatment of acid mine drainage: The relative role of adsorption and co-precipitation. *Applied Geochemistry,* 37**,** 57-63.

PARKER, A. J. 1986. Tectonic development and metallogeny of the Kanmantoo Trough in South Australia. *Ore Geology Reviews,* 1**,** 203-212.

POLLOCK, M. V., SPRY, P. G., TOTT, K. A., KOENIG, A., BOTH, R. A. & OGIERMAN, J. 2018. The origin of the sediment-hosted Kanmantoo Cu-Au deposit, South Australia: Mineralogical considerations. *Ore Geology Reviews,* 95**,** 94-117.

PRISA, M. E. R.-. 2005. Notes on the Brukunga Pyrite Mine. *In:* SA, P. I. A. R. (ed.). Goverment of South Australia.

SHABALALA, A. N., EKOLU, S. O., DIOP, S. & SOLOMON, F. 2017. Pervious concrete reactive barrier for removal of heavy metals from acid mine drainage - column study. *J Hazard Mater,* 323**,** 641-653.

TAYLOR, J., PAPE, S. & MURPHY, N. 2005. A summary of passive and active treatment technologies for acid and metalliferous drainage (AMD). *5th Australian workshop on Acid Mine Drainage,* Fremantle, Australia.

UVAROVA, Y. A., GAZLEY, M. F., CLEVERLEY, J. S., BAENSCH, A., LAWIE, D. & LEGRAS, M. 2016. Representative, high-spatial resolution geochemistry from diamond drill fines (powders): An example from Brukunga, Adelaide, South Australia. *Journal of Geochemical Exploration,* 170**,** 1-9.

WORRALL, R., NEIL, D., BRERETON, D. & MULLIGAN, D. 2009. Towards a sustainability criteria and indicators framework for legacy mine land. *Journal of Cleaner Production,* 17**,** 1426-1434.

Appendix A – Results from Column Experiments